

Numerical Analysis of Melting and Melt Flow Behaviour in Extrusion Deposition Process

A Thesis Submitted to
Indian Institute of Technology, Hyderabad
In Partial Fulfillment of the Requirements
for the Degree of
Master of Technology
by
Aniket Karandikar
(ME14MTECH11017)



भारतीय प्रौद्योगिकी संस्थान हैदराबाद
Indian Institute of Technology Hyderabad

Department of Mechanical and Aerospace Engineering

June 2016

Declaration

I declare that this written submission represents my ideas in my own words, and where ideas or words of others have been included, I have adequately cited and referenced the original sources. I also declare that I have adhered to all principles of academic honesty and integrity and have not misrepresented or fabricated or falsified any idea/data/fact/source in my submission. I understand that any violation of the above will be a cause for disciplinary action by the Institute and can also evoke penal action from the sources that have thus not been properly cited, or from whom proper permission has not been taken when needed.

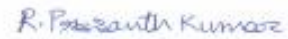
A handwritten signature in blue ink, appearing to read 'Aniket', is written over a horizontal line.

ANIKET KARANDIKAR

ME14MTECH11017

Approval Sheet

This report entitled '**Numerical Analysis of Melting and Melt Flow Behaviors in Extrusion Deposition Process**' by Aniket Karandikar (ME14MTECH11017) is approved for the degree of Master of Technology from IIT Hyderabad



Dr. R. Prasanth Kumar

Examiner

Dept. of Mechanical and Aerospace Engineering

IITH



Prof. N. Venkata Reddy

Advisor

Dept. of Mechanical and Aerospace Engineering

IITH



Dr. Kishalay Mitra

Chairman

Dept. of Chemical Engineering

IITH

23/06/2016

ACKNOWLEDGEMENTS

I would like to take this opportunity to express my deep sense of gratitude and profound regards to Prof. N. Venkata Reddy for his supervision, encouragement and constant motivation. This work would not have been completed successfully without his support. I sincerely thank him for all his support throughout this work.

I express my sincere regards to all the faculty members of Mechanical and Aerospace engineering department, IIT Hyderabad, for all their support, guidance and valuable suggestions. I deeply thank them for the technical lessons in the difficult subject areas which otherwise would be very difficult to learn.

I would like to thank the entire 2014 batch of Integrated Design and Manufacturing, for their priceless help in studies. I would like to thank the non teaching staff of the manufacturing lab for their constant support.

I would like to thank all my friends and classmates for being an important part of my hostel time in both good and bad situations and making my stay at IIT Hyderabad a memorable one.

I am blessed to have such caring parents. I extend my deepest gratitude to my family, for their endless motivation, invaluable support and love .

I am grateful to the Almighty God and at last, but not the least, I am thankful to everyone and everything that helped me directly or indirectly to complete this work.

Aniket Karandikar

ABSTRACT

The Extrusion Deposition Process is a recently developed additive manufacturing process. In this process, an Archimedean screw placed in a heated barrel is used to melt and feed the polymer. The part is fabricated by depositing the molten polymer in layer by layer fashion. The surface finish and strength of the parts fabricated by Extrusion deposition process depend mainly on the temperature and the viscosity polymer coming out of the extruder. The viscosity and temperature of polymer melt depend on the melting process and the flow of molten polymer in the extruder. Melting of polymer is a complex phenomenon which changes significantly with material properties and process parameters. Accurate prediction of melting process requires complex heat and mass transfer analysis. Development of a generalized model to accurately capture the effect of all parameters and material properties has been proven to be a complicated job. Due to the lack of a generalized model, numerical study is required to accurately model the melting process in the extruder. Present study is based on the numerical predictions to accurately model the melting of the polymer and to study the effect of the process parameters on the melting process and melt temperature.

Present study contains a numerical model developed to accurately model the melting of the polymer in the single screw extruder. The model has been verified by comparing with the available experimental results. The present study also contains a parametric study to understand the effect of the process parameters on the melting of the polymer. In this study, the barrel temperature, the screw speed and the feed rate are varied to understand the changes in the melting mechanism and the flow of the molten polymer. Numerically predicted melt profiles and solid fractions at various lengths of the screw are presented. The bulk mean temperature of the polymer coming out of the extruder is studied for each variation as it significantly affects the bond strength and surface finish of an additive manufacturing product.

LIST OF CONTENTS

Chapter 1 : Introduction	1
1.1 Overview of FDM and its development	2
1.2 Extrusion Deposition process	4
1.3 Literature review	6
1.4 Effect of melt temperature on surface finish	8
1.5 Effect of melt temperature on bond strength	9
1.6 Scope and Objective	10
1.6.1 Objective of the present work	10
Chapter 2 : Single screw extruder	11
2.1 Construction of the flow channel	12
2.1.1 Feed zone	12
2.1.2 Melting zone	13
2.1.3 Metering zone	13
2.2 Melting mechanism	13
2.3 Design of the extruder	16
Chapter 3 : Numerical analysis of the melting process	17
3.1 Assumptions	18
3.2 Continuity equation	19
3.3 Momentum conservation equation	19
3.4 Energy conservation equation	22
3.5 Melting model	23
3.6 Constitutive model	25
3.6.1 User Defined Function for Cross WLF model	28
3.7 Mesh generation	29
3.8 Boundary conditions	31

3.9 Solution method	33
Chapter 4 : Results and Discussion	34
4.1 Mesh convergence	34
4.2 Model validation	41
4.2.1 Boundary conditions	42
4.3 Parametric study	46
4.3.1 Variation of barrel temperature	47
4.3.2 Variation of flow rate	52
4.3.3 Variation of screw speed	55
Chapter 5 : Conclusion and Future work	59
5.1 Conclusion	59
5.2 Scope of the future work	60
References	62

LIST OF FIGURES

Fig. 1.1 Fused deposition modelling (a) Process (b) Buckling	2
Fig. 1.2. Multiphase Jet Solidification	3
Fig. 1.3: Extrusion deposition process	5
Fig. 1.4: Variation of surface quality with melt temperature	9
Fig. 2.1 Details of the extruder screw	12
Fig. 2.2 Maddock Melting mechanism.....	14
Fig. 2.3 The cross section of flow channel at (a) Feed zone and (b) Metering zone	16
Fig. 2.4 Nomenclature of the extrusion screw	16
Fig. 3.1 (a) Helical channel and (b) Unwounded helical channel.....	19
Fig. 3.2 Specific volume vs Temperature for ABS resin	27
Fig. 3.3 Tetrahedral mesh applied on the flow channel.....	30
Fig. 3.4 Relative motion between screw and barrel and the boundary conditions	31
Fig. 3.4 Boundary conditions in (a) wounded and (b) unwounded helical channels.....	32
Fig. 4.1 Meshes used for convergence study - (a) 0.5X mesh, (b) 1X mesh, (c) 2X mesh.....	35
Fig. 4.2 Melt profile at various axial lengths (a) 1X mesh (b) 2X mesh	38
Fig. 4.3 Temperature profile at various axial lengths (a) 1X mesh (b) 2X mesh.....	39
Fig. 4.4 Comparison of solid fractions along the axial length	40
Fig. 4.5 Comparison of axial pressure along the axial length	40
Fig. 4.6 (a) Melt profile observed in experiments (Altinkaynak et. al.)	
(b) Melt profile predicted by the numerical analysis.....	43

Fig. 4.7 Variation of axial pressure observed in simulations compared with that in experiments by Altinkaynak et. al.	44
Fig. 4.8 Comparison of the axial pressures predicted by the numerical simulations and the experimental and numerical results reported by Altinkaynak et. al.	44
Fig. 4.9 Predicted melting in the melting section of the extruder at the barrel temperature of (a) 230 ⁰ C (b) 250 ⁰ C (c) 270 ⁰ C	48
Fig. 4.10 Predicted temperature profiles in the melting section of the extruder at the barrel temperature of (a) 230 ⁰ C (b) 250 ⁰ C (c) 270 ⁰ C	49
Fig. 4.11 Predicted solid fraction along the axial length in the melting section of the extruder at the barrel temperature of 230 ⁰ C, 250 ⁰ C and 270 ⁰ C	50
Fig. 4.12 Predicted bulk mean temperature in the metering zone for barrel temperatures of 230 ⁰ C, 250 ⁰ C and 270 ⁰ C	51
Fig. 4.13 Comparison of melt profiles at various flow rates (a) 75 kg/hr (b) 60 kg/hr (c) 45 kg/hr	53
Fig. 4.14 Predicted solid fraction along the axial length for flow rates of 45 kg/hr, 60 kg/hr and 75 kg/hr.....	54
Fig. 4.15 Variation of axial pressure developed along the axial length of flow channel	54
Fig. 4.16 Comparison of melt profiles at various flow rates (a) 45 rpm (b) 60 rpm (c) 45 rpm.....	56
Fig. 4.17 Variation of solid fraction along the length of melting zone for various screw speeds .	57
Fig. 4.18 Variation of axial pressure along the axial length for various screw speeds.....	57
Fig. 4.19 Variation of bulk mean temperature in the metering zone for various screw speeds...	58
Fig. 4.20 Variation of bulk mean temperature in the metering zone for various flow rates	58

LIST OF TABLES

Table 3.1 Physical properties of ABS melt	26
Table 3.2 The values of Cross WLF viscosity model parameters for ABS	28
Table 4.1 Mesh comparison.....	36
Table 4.2 Axial pressure developed at the end of the metering section	50

NOMENCLATURE

ABS	Acrylonitrile Butadiene Styrene
A_c	Cross sectional area of the channel
C_p	Specific heat at constant pressure
D	Outer diameter of the screw
e	Internal energy of the fluid
f_i	Body force in i^{th} direction
h	Sensible enthalpy of the fluid
h_{ref}	Reference enthalpy of the fluid
H	Enthalpy of the fluid
H_f	Depth of channel in feed section
H_m	Depth of channel in metering section
k	Thermal conductivity of the fluid
\dot{m}	Mass flow rate of the polymer
N	Screw speed
P	Pressure of the fluid
P_s	Pitch of the screw
\dot{q}	Volumetric heat generation of the fluid
R_c	Compression ratio
T	Temperature of the fluid
T_{ref}	Reference temperature of the fluid
T_g	Glass transition temperature of the polymer
T_m	Melting temperature or Flow temperature of the polymer
T_b	Barrel temperature
T_0	Inlet temperature of the polymer
T_{bm}	Bulk mean temperature of the polymer melt
u	Velocity of polymer in the width direction
V	Velocity of the polymer
v	Velocity of polymer in the thickness direction

V_b	Barrel velocity
V_{bz}	Barrel velocity along the flow channel
V_{bx}	Barrel velocity along the width of the channel
w	Velocity of polymer along the unwounded flow channel
\bar{w}	Average flow velocity along the channel
ΔH	Latent heat of the polymer
β	Liquid fraction
$\dot{\gamma}$	Shear rate
θ_n	Helix angle
λ	Second coefficient of viscosity
μ	Viscosity or Coefficient of viscosity
μ_0	Zero shear viscosity of the polymer
ρ	Density of polymer
τ_{ij}	Stress in the j direction acting on a plane perpendicular to i direction
τ, n, E, A_1, A_2	WLF model constants for ABS

CHAPTER 1

INTRODUCTION

Additive manufacturing is an advanced manufacturing process used to manufacture 3D parts from a CAD file by depositing material in layer by layer fashion. The part is built by depositing material instead of removing material from bulk giving the process a distinct advantage of forming any complex geometry which cannot be easily fabricated by using traditional machining process. Additive manufacturing process is completely end product dependent. This process requires no product dependent tooling hence it is the most suited to produce the customized products. The absence of specific tooling also reduces the overall product development time and the production is rapid. Due to the ability of producing customized products at a faster rate, this process is also known as Rapid Prototyping. Additive manufacturing finds its wide applications in aerospace and biomedical industries where producing the intricate parts by traditional manufacturing processes can be costly and time consuming. Additive manufacturing finds its advantage in producing the geometries which are limited by conventional manufacturing processes. The product can be fully design driven instead of depending on design for manufacturing. This provides high degree of design flexibility and production customization.

In additive manufacturing, the object is created in form of a STL file. This STL file is then sliced in a chosen orientation in a number of layers having specific thickness. The part orientation has effect on strength, surface finish and other properties of the part. Then each layer is deposited to obtain a 3D object. There are many sub-categories in additive

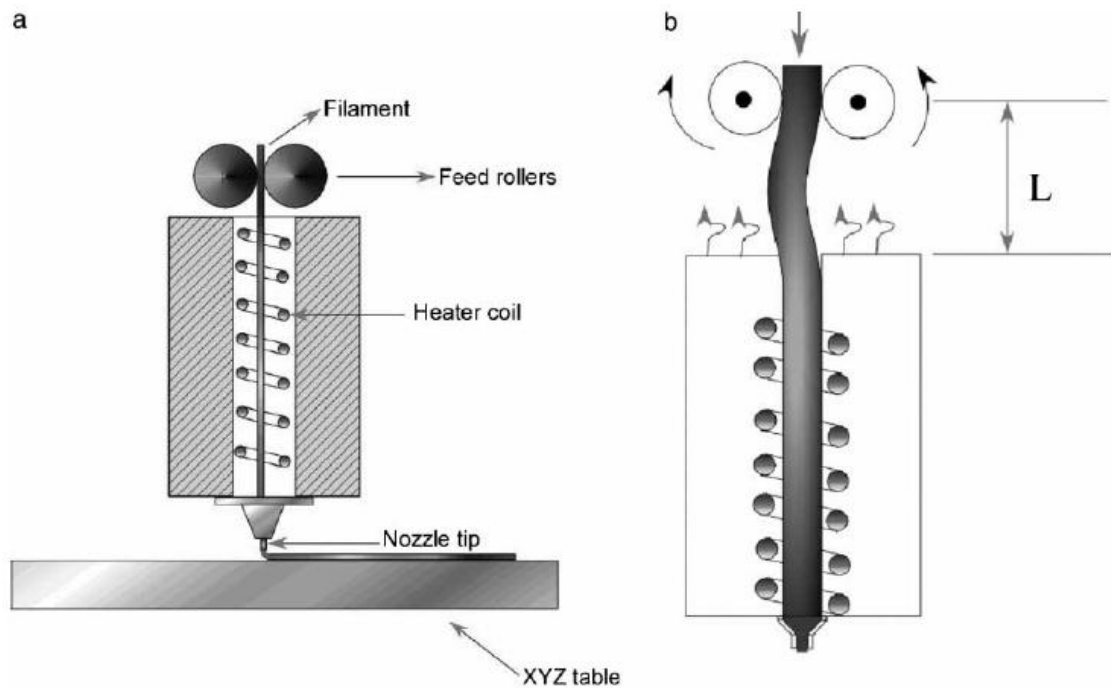


Fig. 1.1 Fused deposition modelling (a) Process (b) Buckling [1]

manufacturing. These processes include fused deposition modelling, direct metal deposition, selective laser sintering, inkjet modelling, stereolithography, etc. Each process has its own advantages and disadvantages depending on the materials and process parameters. The present work focuses on the studies on extrusion deposition process which is a modification of fused deposition process.

1.1 Overview of FDM and its development:

Fused deposition modelling was first developed by Stratasys Inc. in 1990s. The process is now widely used for rapid prototyping. FDM uses thermoplastics due to their ability to melt and solidify at relatively lower temperatures as compared to the other materials. FDM can use a variety of polymers such as Polystyrene, Acrylonitrile Butadiene Styrene (ABS), Polycarbonates, etc.

Fig. 1.1 shows a schematic of fused deposition modelling process [1]. In FDM a polymer filament is fed into the heater with help of feed rollers from the top of the heater. The heater consists of heating coils which melt the filament. Temperature of the heater is kept just above the melting point of the polymer. The liquefied polymer is pushed forward

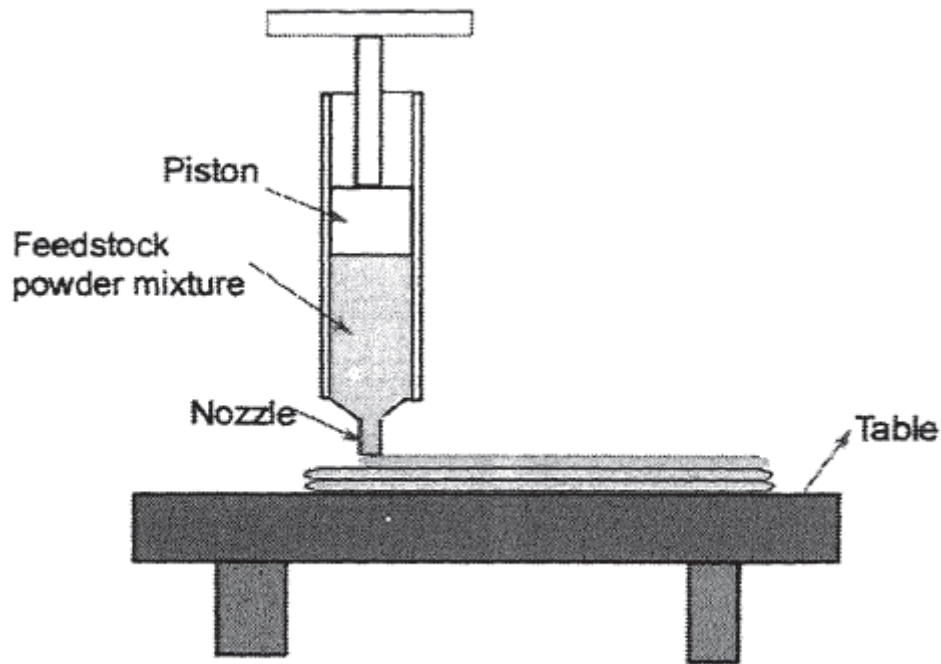


Fig. 1.2. Multiphase Jet Solidification [1]

by the solid portion of the polymer. The molten polymer is extruded from the nozzle. The whole assembly is mounted on a platform. The platform can move in X, Y and Z directions. The material flow through the nozzle remains continuous. The layer by layer deposition of material results in the final product. This process has a few variants where the polymer is replaced by mixture of polymers with ceramics or metals. However there are limitations associated with this process.

One of the major limitations associated with the FDM process is the buckling of the filament [2]. As shown in fig. 1.1, as the solid filament pushes the liquefied polymer, there is a possibility of buckling the liquefied part. This issue can interrupt the whole process making the human intervention necessary. Another limitation is the difficulty in making the filaments when dealing with ceramics. To overcome these limitations, the process is modified. The new process is called Multiphase Jet Solidification which is developed by IFAM, Bremen, Germany.

Fig. 1.2 shows Multiphase Jet Solidification (MJS) process which is a developed version of FDM [1]. In MJS process, the heating barrel and feed rollers are replaced by an

piston cylinder extruder. The feedstock consists of a mixture of polymer and metal powder or ceramic powder. This feedstock is heated beyond the melting temperature of the polymer and then pushed through the nozzle with help of the piston. The rest of the process remains similar to the FDM process. There is a major disadvantage present with the process that the feedstock is limited. Limited number of parts can be produced without replacing the feedstock. This also restricts the maximum size of the parts.

1.2 Extruder Deposition process:

Extrusion Deposition process was developed to overcome the limitations of Multiphase Jet Solidification process that is to get a continuous polymer outcome from the nozzle. The process was first developed by Bellini et. al. [3] for the tissue scaffold fabrication. They used an Archimedean screw to extrude the molten polymer. The extruder consists of a Archimedean screw and a heating barrel. The polymer is fed in the extruder from the top and as the screw rotates, it conveys the polymer to the nozzle. Simultaneously the barrel is heated which melts the polymer present in the screw extruder. The polymer melt is taken out from the nozzle and deposited on a moving platform to get the final object.

The extruder developed by Bellini et. al. [3] had several problems. The extruder used a metal pipe to feed the pellets. Aggregation of pellets was observed at the entrance of the extruder. They used a screw with uniform pitch and constant channel depth. This resulted in air entrapment in the extruder. In this screw extruder, one end of the screw is unsupported. When a radial pressure gradient is developed in the screw, the screw deflects like a cantilever.

The problems in this extruder were solved by Reddy et. al. [1]. They used a ceramic pipe instead of a metal pipe to stop aggregation of pellets at the entry. They used a spider bearing at the end of the extruder to support the screw and restrict the deflection of the screw. They used an extruder screw with varying channel depth. The screw had three sections, namely feed section, melting section and metering section. The depth of channel more in the feed section than the metering section. It gradually decreases in the melting

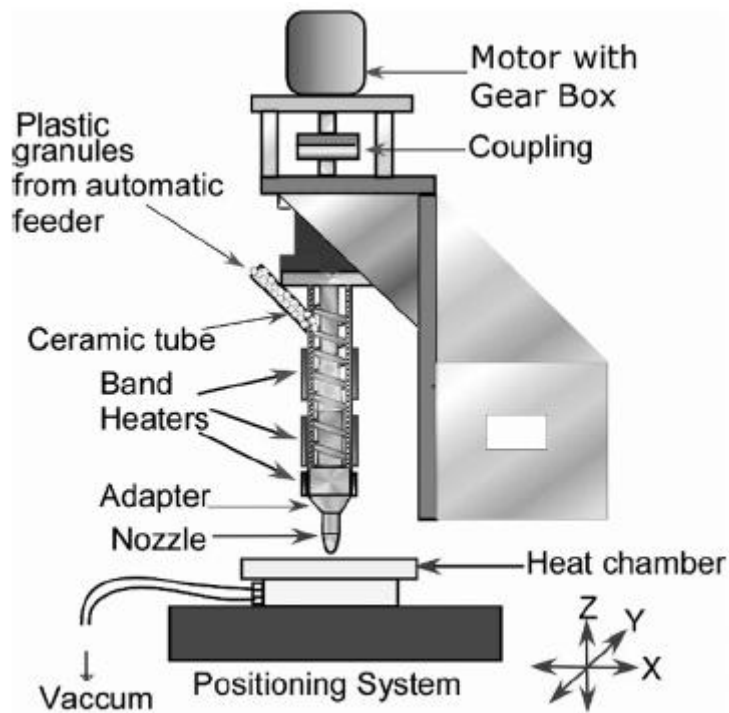


Fig. 1.3: Extrusion deposition process [1]

section. The major advantage of this design is that it creates a compressive zone in the melting section. As polymer moves towards melting section, it starts compressing the polymer which prevents the air from entering in the melting section. Thus the problem of air entrapment is solved.

The extrusion deposition system consists of a screw and barrel assembly, heaters, a motor to drive the screw, thermocouples, controls and a positioning system. The assembly is shown in fig. 1.3 [1]. The extruder consists of an Archimedean screw fitted in a long barrel. The barrel is open from one side. An adapter and nozzle assembly is attached on the other end of the barrel. The adapter provides housing for the breaker plate. The barrel has a 45° inclined hole on the top portion in which feed pipe is connected. One end of the screw is connected to the motor and the other end rests inside the barrel on a breaker plate. The breaker plate consists of four holes and a conical section. The extruder screw rests on the conical section. The holes make the path for the polymer melt. The purpose of this design is to make polymer flow irrotational as the melt comes out of the screw and flows towards the nozzle. Two taper roller bearings are mounted on the motor side of the screw to take the

axial loads. The whole assembly is mounted on a rigid support connected to a positioning system.

Barrel and adapter are heated by ceramic band heaters. Heaters are controlled by the PID controllers with help of relays. The controllers take temperature input from the thermocouples. The feeding is done by a screw feeder driven by another DC motor. The motor voltage can be varied to change the feed rate.

Extrusion deposition process is capable of producing larger parts as compared to FDM and its other variants. The process can handle a variety of polymers and produce a wide range of products by layered deposition. However it is clear that the quality of product depends on the polymer melt behaviour as shown by Reddy et. al. [1].

1.3 Literature review:

The quality of final product made by extrusion deposition process highly depends on the quality of polymer coming out of the extruder. The polymer quality highly depends on the melting process in the melting section of the extruder and the mixing process in the metering section of the extruder. Tadmor and Klein [4] and Sastrohartono et. al. [5] found that the main parameters affecting the polymer quality are the screw speed, barrel temperature and material feed rate.

In the past few decades a number of analytical and experimental studies have been carried out to find the melting process in the extruder. Maddock [6] performed a series of screw freezing experiments to understand the melting in the screw extruder. He proposed the first melting model for the polymer extrusion which is discussed in detail in chapter 2. A numerous experimental studies have been carried out which mostly confirmed Maddock's model (Cox et. al. [7], Marshall and Klein [8], Tadmor et. al. [9], Kulas and Thorshaug [10]). However Kulas and Thorshaug [10] performed experiments with PVC and found that the melt pool shifts towards the active flight as screw speed increases. These results suggest that there is a possibility of more than one melting mechanism as the material and process parameters vary.

Tadmor et. al. [9] developed the analytical model for the melting of polymer in the extruder. They performed the heat and mass balance on the melt pool formed above the solid bed to obtain the size of the solid bed. This model was further developed by Tadmor and his colleagues (Tadmor and Klein [4], Tadmor and Gogos [11]). The new improved model used the temperature and shear rate dependent viscosity model to accurately predict the solid bed profile and the melting rate.

Mount and Chung [12] experimentally studied the effect of barrel temperature, pressure and flow velocity on melting of several polymers. They compared the melt profile and found that the experimental results did not agree with results predicted by Tadmor's model. However the first Tadmor's model predicts the solid bed accurately due to its assumption of constant solid bed velocity. Even though the predictions are accurate for uniform screw channel, they tend to be unrealistic in case of tapered channels. For tapered channels, Tadmor's first model predicts solid bed widths larger than the channel widths to satisfy the continuity of flow. Even though Tadmor's melting models give an idea about the melting in the extruder, there is no single model to predict the melting profile, solid bed profile, shear rate and their behaviour with variation in process parameters.

Because of the lack of accurate melting model, the accurate prediction of melt profile and melting process can only be obtained numerically by solving the governing equations of flow, momentum and energy coupled with appropriate constitutive models. The numerical analysis of melting was first attempted by Viriyayuthakorn and Kassahun [13]. Their results show that at the entry of the compressive melting section of the screw, the solid bed profile is surrounded by the polymer melt from all four sides which is not in agreement with the experimental results reported by Maddock [6]. Viriyayuthakorn and Kassahun applied standard Galerkin formulation on the governing equations. However for such convection dominant problems, Galerkin formulation gives oscillating and inaccurate solution. For such problems, upwind schemes must be applied to obtain steady and accurate solutions which was not done by Viriyayuthakorn and Kassahun.

Griffith [14] was the first to solve the governing equations for incompressible fluid flow inside an extruder. He used the boundary condition as screw temperature equal to the barrel temperature. He found the temperature and velocity profiles same as those in a couette flow i.e. a drag flow between two infinite parallel plates. A numerical analysis to

estimate the polymer quality at the output was done by Syrjala [15]. He found out the effect of barrel temperature, flow rate and screw speed on the properties of polymer output. However he assumed the polymer to enter the metering zone in a completely molten state and carried out the analysis on metering zone only. He proposed a marching solution to solve the parabolic equations in a plane normal to the flow direction to obtain the velocity and temperature profiles.

Syrjala [16] performed a three dimensional analysis on an unwound cross section of constant depth. He assumed a fully developed flow in the channel and proposed a space marching solution. He assumed constant solid bed velocity calculated from the mass flow rate at the inlet of the channel. He also assumed negligible viscous heating. He obtained the results close to the predictions of Tadmor's model. However this approach cannot be used in tapered screw channels since the assumption of fully developed cross section is no longer valid in this case.

The most recent numerical study towards understanding the melting process in the compressive section of the extruder was done by Altinkaynak et.al. [17]. They performed a full three dimensional analysis on the melting and metering zones of the single screw extruder. They studied the effect of process parameters and material properties on the melting profile. Their results were in good agreement with the experiments. However they did not discuss the effect of process parameters on the quality of polymer coming out of the extruder.

1.4 Effect of melt temperature on surface finish:

As the temperature of melt increases, its viscosity decreases. Polymer melt flows better at higher temperatures. Vasudevarao et. al. [18] found that if material is deposited at a high temperature the material deposited along one raster spreads wider as shown in fig. 1.4 [19]. This leads to reduction in peak to valley height between adjacent roads and produces better surface finish. Horvath et. al. [20] experimentally verified this effect of melt temperature on surface finish.

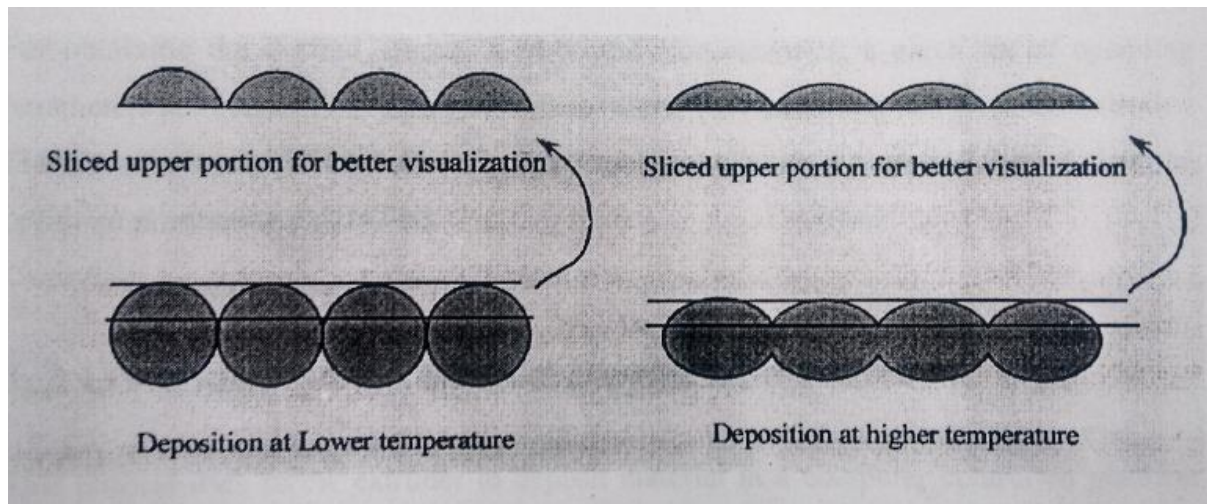


Fig. 1.4: Variation of surface quality with melt temperature [19]

1.5 Effect of melt temperature on bond strength:

The bonding between two roads of a part depend on the temperature at which the roads are deposited. If the temperature is well above the glass transition temperature the polymer chains of the two contacting road interfaces diffuse into each other creating a bond in between the two roads. The bond strength depends on the diffusion which again depends on the melt temperature. Bonding becomes stronger as the melt temperature increases. Ahn et. al [21] found that lower melt temperature results in weak bonding between two roads. This weak bond formed at the edge of the part leads to stress concentration zone which reduces the part strength.

The present work consists of a detailed numerical study of the flow of fluid and solid mixture in the melting and metering section of the extruder.

1.6 Scope and Objectives:

The surface quality and strength of a product made by extrusion deposition process highly depends on the quality of polymer coming out of the extruder. In order to get high quality products, it is of utmost importance to study the melting process and the effect of the process parameters on the melting of the polymer. The main operating parameters that affect the melting process and melt quality are the barrel temperature, feed rate and screw speed.

Based on the literature review, it is clear that there is no single model which can predict the melting profile accurately. However the same thing can be predicted numerically with greater accuracy than the mathematical model. The current study focuses on the melting and flow of polymer in the melting and metering sections of the extruder.

1.6.1 Objectives of the present work:

1. The present study consists of a full three dimensional numerical analysis of the melting process and two phase flow in the single screw extruder.
2. Governing equations of continuity, momentum and energy are coupled with a Cross-WLF constitutive model for temperature and shear rate dependent viscosity. The solution is obtained by a semi implicit scheme by using the upwinding technique.
3. The present work also contains the study of effect of process parameters (barrel temperature, screw speed and feed rate) on the melting process and the quality of polymer melt.

CHAPTER 2

WORKING PRINCIPLE OF SINGLE SCREW EXTRUDER

In Fused Deposition Modelling, continuous production of parts was difficult due to buckling of the filament. Extrusion Deposition process was developed to overcome this limitation of Fused Deposition Modelling. In Extrusion deposition process, the polymer is melted in a heated barrel and extruded with help of an Archimedean screw. The process consists of an Archimedean screw, a long barrel to accommodate the screw, an electric motor to drive the screw, ceramic band heaters to heat the barrel, a nozzle, a spider bearing, an adapter, a XYZ positioning platform and a control system. The polymer is fed to the extruder in form of pellets through a ceramic pipe with help of a screw feeder. This polymer is simultaneously fed and melted inside the barrel. Molten polymer comes out from the nozzle and it is deposited on the platform having motion in the three directions.

The properties of the fabricated part depend on the temperature and viscosity of the molten polymer coming out of the extruder nozzle. Hence it is important to study the melting process and the flow of polymer melt in the extruder in order to predict the polymer quality.

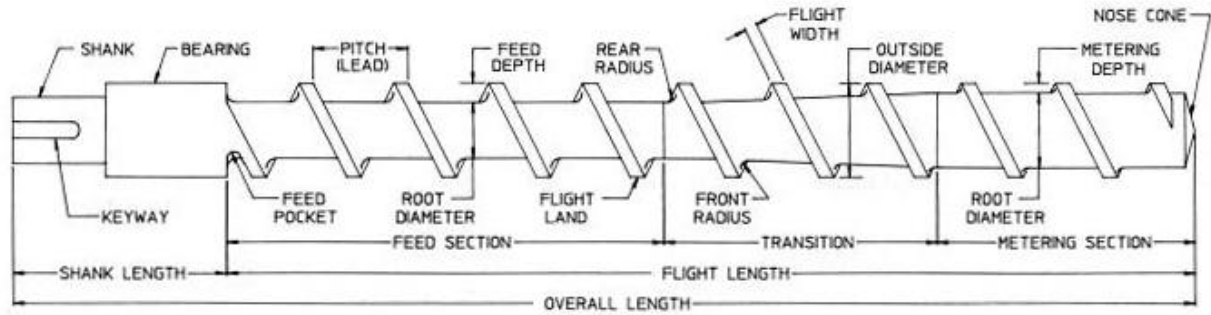


Fig. 2.1 Details of the extruder screw [11]

2.1 Construction of the flow channel:

The Archimedean screw forms the flow path for solid and molten polymer. The main functions of the screw are as follows

- To accommodate the polymer pellets coming from the screw feeder into the feed section of screw.
- To melt the polymer pellets completely.
- To feed the polymer pellets to the nozzle through the rotation of the screw.
- To pressurize the polymer melt to overcome the pressure rise in the nozzle.

On the basis of channel depth, the Archimedean screw is divided into three parts namely the feed, melting and metering zone as shown in fig. 2.1 [11].

2.1.1 Feed zone:

Feed zone of the screw is the section with constant channel depth. Polymer coming to the extruder is in the form of solid pellets having air entrapped between them. Hence density of polymer pellets is less than that of the polymer melt. Hence to accommodate the same volume of the polymer with additional volume of air, depth of feed zone is kept more than the depth of the remaining parts of the channel.

2.1.2 Melting zone:

The melting zone or the compressive zone is the tapered part of the extruder. In this zone, the channel depth gradually reduces from maximum to minimum depth. The bulk density of polymer is much less than the melt density. Hence it is essential to compress the polymer which is done due to the gradual reduction in channel depth. This compression is necessary to ensure that the entrapped air does not pass through the melting zone and cause the formation of air bubbles in the polymer melt. In this zone, polymer transits from the solid to liquid form and both phases of polymer exist.

2.1.3 Metering zone:

The final zone of the Archimedean screw is the metering zone. The channel depth is constant in this zone which is also the minimum channel depth of the screw channel. The main function of the metering zone is to homogenize the polymer melt and feed it to the nozzle.

2.2 Melting mechanism:

Melting mechanism in the compression zone of the extruder has been a topic of study for many researchers. Maddock [6] first carried out the screw freezing experiments to investigate the melting in the screw extruder. He mixed 1-2% of a coloured resin in the polymer, which had a higher melting point than the polymer. Hence the coloured resin remains solid while the polymer melts first. During the melting process, coloured resin remains the part of solid bed giving it a characteristic colour and making it visually distinguishable from polymer melt. In the screw freezing experiments, the flow in the screw channel is made stable and then the extruder is stopped and polymer melt is allowed to solidify. Solid polymer is taken out from the screw channel and sliced to observe the solid bed profile. Based on these observations, Maddock proposed a melting model for single screw extrusion.

In the melting zone of the extruder, polymer is assumed to enter in the form of pellets. The compressive zone prevents air to go through it and form air bubbles in the melt. As the polymer flows in the melting zone, its temperature starts increasing due to heat

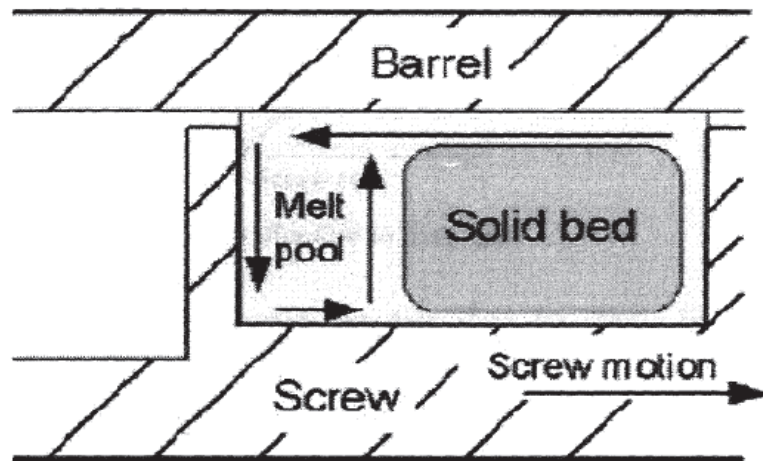


Fig. 2.2 Maddock Melting mechanism [19]

conduction from the barrel. As the temperature rises above the glass transition temperature, the polymer starts melting. As the temperature increases, the viscosity of polymer melt decreases. As polymer melt starts flowing, viscous heat generates and supports the melting process further. Viscous shear heating has two sources, one from the polymer melt flow and the other from the viscous heating taking place at the small clearance between screw flight and the barrel. Shearing takes place due to the motion of one polymer layer relative to the barrel surface or the other polymer layer. Increase in the shear reduces the viscosity of polymer melt. This is known as the shear thinning behaviour which is exhibited by most of the polymers. High shear rates and high polymer viscosity in the extruder make the viscous shear heating the major factor in heating and melting of the polymer.

As the polymer enters the melting zone, it is pushed forward by the trailing flight. Due to the heating of barrel, heat is conducted to the polymer. This heat melts the polymer adjacent to the barrel and forms a thin film of polymer melt between the barrel and the solid bed of the polymer. The polymer melt in the thin film flows towards the leading flight due to the relative motion between barrel and screw. Viscous heat is generated during this flow which supports further melting of the polymer. Due to the melt flow towards the leading flight, a melt pool is generated near the leading flight. Fig. 2.2 shows the melting of polymer in the channel [19].

A small amount of melt flows in the clearance between the barrel and the screw flights creating more viscous heating. As the polymer progresses in the channel, the cross section area goes on reducing. The screw forces solid bed against the barrel wall. This results in further melting of the bed. Continuous movement between barrel wall and solid bed conveys the melt formed between the two to the leading flight. This flow increases the size of the melt pool. As the polymer progresses in the channel, melt pool size increases while solid bed width decreases. Solid bed thickness nearly remains constant in the process.

Solid bed width, melt film thickness and barrel temperature have significant effect on the melting process. As the solid bed width increases, the surface area between barrel and solid bed increases. Increased surface area accommodates wider polymer melt film which results in more viscous heating. Hence as solid bed width increases, more heat is generated and melting rate increases. For better melting, solid bed width needs to be as large as possible.

Viscous heat generated in the barrel is inversely related to the melt film thickness. As film thickness reduces, the shear rate increases. Increased shear rate causes increased viscous heating resulting in more heat and hence better melting. Clearance between the barrel and screw has a similar effect on melting. Increased clearance due to wearing of screw or barrel increases film thickness and reduces the shear rate. This results in reduction in melting rate of the polymer.

The barrel temperature has a critical role in melting of the polymer. High barrel temperature results in a thicker polymer melt film reducing the shear rate and viscous heating. This reduces the melting rate of solid bed. Melting rate may not be sufficient to ensure complete melting of the polymer before it enters the metering zone. Decreasing the barrel temperature increases the melting rate by increasing the viscous heating.

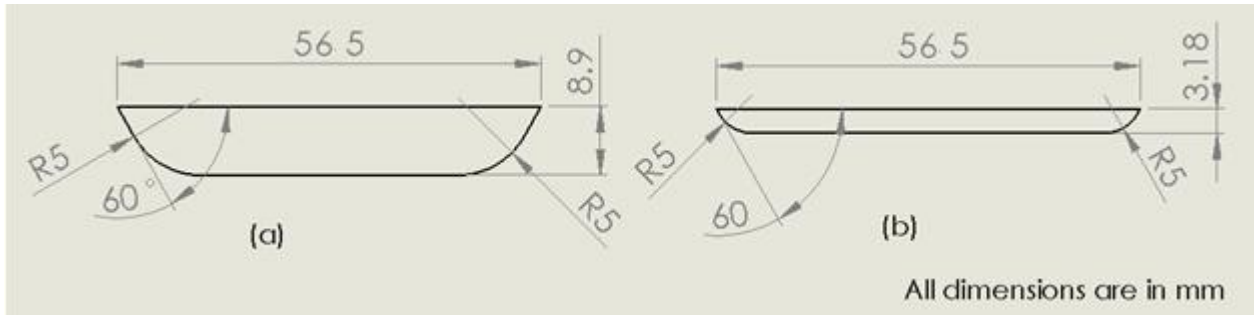


Fig. 2.3 The cross section of flow channel at (a) entry of melting section

(b) exit of melting section

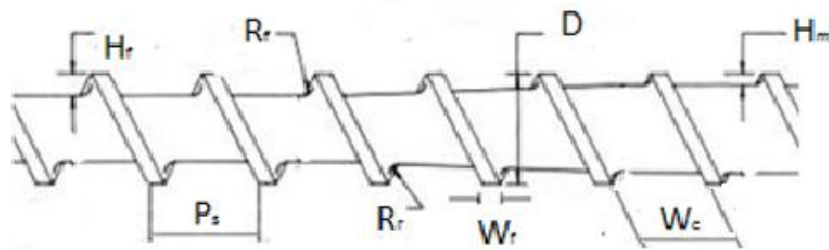


Fig.2.4 Nomenclature of the extrusion screw

2.3 Design of the extruder:

The screw design used for current study has following dimensions:

Outer diameter of screw = $D = 63.5$ mm

Pitch = $P_s = \text{diameter} = 63.5$ mm

Length to diameter ratio = 21

Helix angle = $\theta_h = 17.66^\circ$

Compression ratio, $R_c = \frac{H_f}{H_m} = 2.8$

Depth of channel in feed section = $H_f = 8.9$ mm

Depth of channel in metering section = $H_m = 3.18$ mm

Front corner radius (R_f) = Rear corner radius (R_r) = 5 mm

Width of flights, W_f = 8 mm

Channel width, W_c = 55.5 mm

Fig. 2.3 shows the cross section of the screw at the entry and exit of the melting section. The current design is chosen for simulations as the experimental data is available for this design [17] and it is convenient to validate the design.

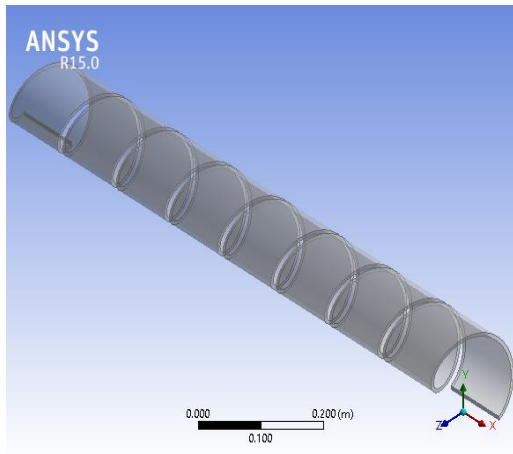
Due to the square pitch threads, it is convenient to measure the length of the screw in terms of the diameter. The current design has the melting section of 8 diameters and metering section of 7 diameters. The axial length is mentioned in terms of diameters in this study.

CHAPTER 3

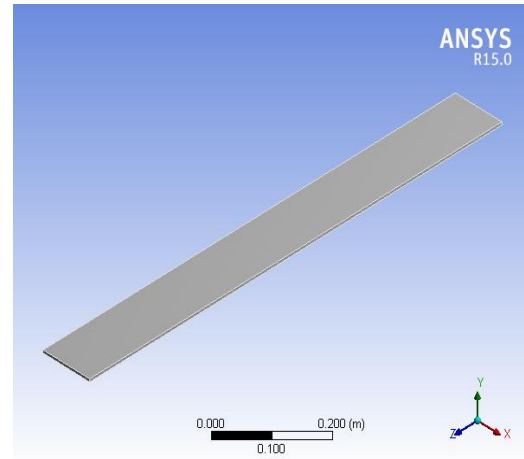
NUMERICAL ANALYSIS OF MELTING PROCESS

The flow in the melting section of the single screw extruder is a multiphase flow involving the solid bed moving forward while simultaneously getting melted. The polymer melt exhibits a complex non-Newtonian compressible viscous flow which is complicated to model analytically. In addition to that some of the polymers are amorphous in nature. As their temperature crosses the glass transition temperature, they start softening. They exhibit a shear thinning behaviour. All these factors make the flow and melting of polymer a complex phenomenon.

Many studies have been done in the past to model the melting process. There are models which predict the solid bed profile or the melting rate independently but there is no single model which can accurately predict the melting process. This is the motivation behind formulating a numerical model for the process. In this chapter, the governing equations for the fluid flow are derived and a constitutive model for compressible shear thinning fluid is coupled with the equations. To simplify the governing equations, some assumptions are made. Simplified governing equations are solved with SIMPLEC algorithm and an upwinding scheme. The mesh generation is also discussed in detail. A commercial code ANSYS FLUENT 15 was used to solve the governing equations.



(a)



(b)

Fig. 3.1 (a) Helical channel and (b) Unwounded helical channel

3.1 Assumptions

1. The flow is steady over the entire length of the melting and metering zones.
2. Velocity variations along z directions are negligible along the channel as compared to those across the channel.
3. The polymer entering in the domain is in solid state and no air is present at the inlet.
4. Radius of channel is much greater than the depth of channel nullifying the curvature effect. Due to this assumption, an unwounded channel can be used instead of a helical channel as shown in fig. 3.1.
5. No slipping occurs at the walls. Screw walls are assumed to be adiabatic.
6. For the convenience, the screw is considered to be fixed and the barrel is assumed to rotate around the screw in the opposite direction so that the relative motion between the two remains the same.
7. The leakage across the clearance is neglected and the viscous heating taking place in the clearance is not taken into the account.
8. Solid polymer at the glass transition temperature is generally treated as a liquid with infinite viscosity. In the numerical method, an infinite value cannot be assigned to a property. Hence an unrealistically high value is assumed and assigned to the viscosity.

3.2 Continuity equation

The general continuity equation is given as

$$\frac{\partial \rho}{\partial t} + \nabla \cdot (\rho V) = 0 \quad (3.1)$$

For steady state flow,

$$\frac{\partial \rho}{\partial t} = 0$$

$$\nabla \cdot (\rho V) = 0$$

Velocity changes in flow direction (z-direction) is negligible as compared to velocity changes in x and y directions. It can be safely neglected from the above equation.

$$\frac{\partial \rho w}{\partial z} = 0$$

$$\frac{\partial \rho u}{\partial x} + \frac{\partial \rho v}{\partial y} = 0$$

$$\frac{\partial \rho u}{\partial x} + \frac{\partial \rho v}{\partial y} = 0 \quad (3.2)$$

This equation can be used as continuity equation for the current solution.

3.3 Momentum conservation equation

The conservation of momentum equation, also known as the Navier Stokes equation is the generalized momentum conservation equation for any fluid flow. It is derived from the Newton's second law of motion. It is written for x direction as

$$\frac{\partial \rho u}{\partial t} + \nabla \cdot (\rho u V) = -\frac{\partial P}{\partial x} + \frac{\partial \tau_{xx}}{\partial x} + \frac{\partial \tau_{yx}}{\partial y} + \frac{\partial \tau_{zx}}{\partial z} + \rho f_x \quad (3.3)$$

where f_x is the body force in x direction.

The shear stress in the above equation can be stated in terms of velocity gradients by using Stoke's assumption. Stokes assumed that

$$\tau_{ii} = \left(\lambda \nabla \cdot V + 2\mu \frac{\partial u_i}{\partial x_i} \right) \quad (3.4)$$

and

$$\tau_{ij} = \mu \left(\frac{\partial u_i}{\partial x_j} + \frac{\partial u_j}{\partial x_i} \right) \quad (3.5)$$

Therefore the above equation can be written as,

$$\begin{aligned} \frac{\partial \rho u}{\partial t} + \frac{\partial \rho u^2}{\partial x} + \frac{\partial \rho uv}{\partial y} + \frac{\partial \rho uw}{\partial z} \\ = -\frac{\partial P}{\partial x} + \frac{\partial}{\partial x} \left(\lambda \nabla \cdot V + 2\mu \frac{\partial u}{\partial x} \right) + \frac{\partial}{\partial y} \left(\mu \left(\frac{\partial u}{\partial y} + \frac{\partial v}{\partial x} \right) \right) + \frac{\partial}{\partial z} \left(\mu \left(\frac{\partial u}{\partial z} + \frac{\partial w}{\partial x} \right) \right) \\ + \rho f_x \end{aligned}$$

For a steady flow,

$$\frac{\partial \rho u}{\partial t} = 0$$

There is no body force acting on the polymer.

$$f_x = 0$$

Change in flow field variables can be assumed negligible along the flow direction as compared to the cross flow direction. Hence there is no significant gradient of any variable along z direction.

$$\frac{\partial \rho u^2}{\partial x} + \frac{\partial \rho uv}{\partial y} = -\frac{\partial P}{\partial x} + \frac{\partial}{\partial x} \left(\lambda \nabla \cdot V + 2\mu \frac{\partial u}{\partial x} \right) + \frac{\partial}{\partial y} \left(\mu \left(\frac{\partial u}{\partial y} + \frac{\partial v}{\partial x} \right) \right)$$

The variable λ is known as the second coefficient of viscosity. It is found experimentally [22] that the value of λ approximately equal to

$$\lambda = -\frac{2}{3}\mu$$

Therefore the equation reduces to

$$\frac{\partial \rho u^2}{\partial x} + \frac{\partial \rho uv}{\partial y} = -\frac{\partial P}{\partial x} + \frac{\partial}{\partial x} \left(-\frac{2}{3} \mu \left(\frac{\partial u}{\partial x} + \frac{\partial v}{\partial y} \right) + 2\mu \frac{\partial u}{\partial x} \right) + \frac{\partial}{\partial y} \left(\mu \left(\frac{\partial u}{\partial y} + \frac{\partial v}{\partial x} \right) \right)$$

$$\frac{\partial \rho u^2}{\partial x} + \frac{\partial \rho uv}{\partial y} = -\frac{\partial P}{\partial x} + \frac{\partial}{\partial x} \left(\frac{4}{3} \mu \frac{\partial u}{\partial x} - \frac{2}{3} \mu \frac{\partial v}{\partial y} \right) + \frac{\partial}{\partial y} \left(\mu \left(\frac{\partial u}{\partial y} + \frac{\partial v}{\partial x} \right) \right)$$

This is the momentum conservation equation for x direction. Similarly the equation for y direction can be written as

$$\frac{\partial \rho v^2}{\partial y} + \frac{\partial \rho uv}{\partial x} = -\frac{\partial P}{\partial y} + \frac{\partial}{\partial y} \left(\frac{4}{3} \mu \frac{\partial v}{\partial y} - \frac{2}{3} \mu \frac{\partial u}{\partial x} \right) + \frac{\partial}{\partial x} \left(\mu \left(\frac{\partial u}{\partial y} + \frac{\partial v}{\partial x} \right) \right) \quad (3.6)$$

For z direction, the equation is given as

$$\begin{aligned} \frac{\partial \rho w}{\partial t} + \frac{\partial \rho w u}{\partial x} + \frac{\partial \rho w v}{\partial y} + \frac{\partial \rho w^2}{\partial z} \\ = -\frac{\partial P}{\partial z} + \frac{\partial}{\partial z} \left(\lambda \nabla \cdot \mathbf{V} + 2\mu \frac{\partial w}{\partial z} \right) + \frac{\partial}{\partial y} \left(\mu \left(\frac{\partial w}{\partial y} + \frac{\partial v}{\partial z} \right) \right) + \frac{\partial}{\partial x} \left(\mu \left(\frac{\partial w}{\partial x} + \frac{\partial u}{\partial z} \right) \right) \\ + \rho f_z \end{aligned}$$

Simplifying the equations with the same assumptions,

$$\frac{\partial \rho w u}{\partial x} + \frac{\partial \rho w v}{\partial y} = -\frac{\partial P}{\partial z} + \frac{\partial}{\partial y} \left(\mu \left(\frac{\partial w}{\partial y} \right) \right) + \frac{\partial}{\partial x} \left(\mu \left(\frac{\partial w}{\partial x} \right) \right) \quad (3.7)$$

This is the equation of momentum conservation in z direction.

3.4 Energy conservation equation

The generalised energy conservation equation for any flow is given in its conservative form as

$$\begin{aligned}
 & \frac{\partial \rho \left(e + \frac{V^2}{2} \right)}{\partial t} + \frac{\partial \rho u \left(e + \frac{V^2}{2} \right)}{\partial x} + \frac{\partial \rho v \left(e + \frac{V^2}{2} \right)}{\partial y} + \frac{\partial \rho w \left(e + \frac{V^2}{2} \right)}{\partial z} \\
 &= \rho \dot{q} + \frac{\partial}{\partial x} \left(k \frac{\partial T}{\partial x} \right) + \frac{\partial}{\partial y} \left(k \frac{\partial T}{\partial y} \right) + \frac{\partial}{\partial z} \left(k \frac{\partial T}{\partial z} \right) - \frac{\partial uP}{\partial x} - \frac{\partial vP}{\partial y} \\
 & - \frac{\partial wP}{\partial z} + \frac{\partial u\tau_{xx}}{\partial x} + \frac{\partial u\tau_{yx}}{\partial y} + \frac{\partial u\tau_{zx}}{\partial z} + \frac{\partial v\tau_{xy}}{\partial x} + \frac{\partial v\tau_{yy}}{\partial y} + \frac{\partial v\tau_{zy}}{\partial z} \\
 & + \frac{\partial w\tau_{xz}}{\partial x} + \frac{\partial w\tau_{yz}}{\partial y} + \frac{\partial w\tau_{zz}}{\partial z} + \rho f \cdot V
 \end{aligned} \tag{3.8}$$

The enthalpy can be written as

$$H = C_p T = e + \frac{V^2}{2}$$

There is no volumetric heat generation in the polymer flow.

$$\rho \dot{q} = 0$$

Also there are no body forces involved.

$$\rho f \cdot V = 0$$

Along the flow direction, the gradients are negligible as compared to the cross flow directions and can be safely neglected from the equation. For steady flow, the simplified equation can be written as,

$$\begin{aligned}
 & \frac{\partial \rho u H}{\partial x} + \frac{\partial \rho v H}{\partial y} \\
 &= \frac{\partial}{\partial x} \left(k \frac{\partial T}{\partial x} \right) + \frac{\partial}{\partial y} \left(k \frac{\partial T}{\partial y} \right) - \frac{\partial uP}{\partial x} - \frac{\partial vP}{\partial y} + \frac{\partial u\tau_{xx}}{\partial x} + \frac{\partial u\tau_{yx}}{\partial y} + \frac{\partial v\tau_{xy}}{\partial x} + \frac{\partial v\tau_{yy}}{\partial y} \\
 & + \frac{\partial w\tau_{xz}}{\partial x} + \frac{\partial w\tau_{yz}}{\partial y}
 \end{aligned}$$

Again by using Stokes' assumption stated in section 3.3, the equation is written as,

$$\begin{aligned} \frac{\partial \rho u H}{\partial x} + \frac{\partial \rho v H}{\partial y} = & k \left(\frac{\partial^2 T}{\partial x^2} + \frac{\partial^2 T}{\partial y^2} \right) - \frac{\partial u P}{\partial x} - \frac{\partial v P}{\partial y} \\ & + \mu \left(2 \left(\frac{\partial u}{\partial x} \right)^2 + 2 \left(\frac{\partial v}{\partial y} \right)^2 + 2 \left(\frac{\partial w}{\partial z} \right)^2 + \left(\frac{\partial v}{\partial x} + \frac{\partial u}{\partial y} \right)^2 + \left(\frac{\partial u}{\partial z} + \frac{\partial w}{\partial x} \right)^2 \right. \\ & \left. + \left(\frac{\partial v}{\partial y} + \frac{\partial w}{\partial y} \right)^2 \right) \end{aligned} \quad (3.9)$$

This is the simplified form of the energy equation.

Here,

$$\dot{\gamma}^2 = 2 \left(\frac{\partial u}{\partial x} \right)^2 + 2 \left(\frac{\partial v}{\partial y} \right)^2 + 2 \left(\frac{\partial w}{\partial z} \right)^2 + \left(\frac{\partial v}{\partial x} + \frac{\partial u}{\partial y} \right)^2 + \left(\frac{\partial u}{\partial z} + \frac{\partial w}{\partial x} \right)^2 + \left(\frac{\partial v}{\partial y} + \frac{\partial w}{\partial y} \right)^2 \quad (3.10)$$

The term $\dot{\gamma}$ is the shear rate and is responsible for the viscous heating of the polymer.

In the five governing equations, six unknowns, namely the temperature, three velocity components, pressure and density are present. One more equation required to obtain a unique solution is obtained from the constitutive model. The continuity equation, the momentum conservation equation and the energy conservation equation are coupled with constitutive model and solved simultaneously to get the solution.

3.5 Melting model

In the melting zone of the extruder, polymer coexists in both solid and molten form. The heat coming from the barrel is split into two parts. One is the heat which is required to raise the temperature of the polymer and the other is the latent heat required to melt the polymer. The ABS is an amorphous polymer which starts softening after reaching a particular temperature called glass transition temperature. In a particular finite volume, the liquid fraction is computed using a melting model as stated in this section.

The latent heat is computed as

$$\Delta H = H - h$$

where h is the sensible enthalpy of the polymer which is given by

$$h = h_{ref} + \int_{T_{ref}}^T C_p \Delta T$$

where h_{ref} is the reference enthalpy

T_{ref} is the reference temperature

C_p is the specific heat at constant pressure

The latent heat can be written in terms of the liquid fraction and the latent heat of the polymer as

$$\Delta H = \beta L$$

The liquid fraction β is defined as

$$\beta = 0 \text{ if } T < T_g$$

$$\beta = 1 \text{ if } T > T_m$$

$$\beta = \frac{T - T_g}{T_m - T_g} \text{ if } T_g < T < T_m \quad (3.11)$$

3.6 Constitutive model

For current study, ABS is chosen as the material. Physical properties of ABS reported by McKeen [23] are given in table 3.1. It is known that the values of specific heat and thermal conductivity are the functions of temperature. However the change in these values does not affect the process significantly and hence it is safe to consider them as constant.

Property	Value	Unit
Specific heat (C_p)	2345	J/Kg-K
Thermal conductivity (K)	0.18	W/mK
Glass transition temperature (T_g)	100	$^{\circ}\text{C}$
Flow temperature (T_m)	160	$^{\circ}\text{C}$
Latent heat of melting (ΔH)	256.36	J/Kg

Table 3.1 Physical properties of ABS melt

ABS is an amorphous polymer which changes its phase gradually when heated above the glass transition phase. The density change of ABS is linear as the temperature varies linearly. The variation of specific volume of ABS with temperature was given by McKeen [23] as shown in fig. 3.2. From the reported data, the density can be formulated as a piecewise linear function of temperature.

$$\rho = \begin{cases} 1034 - 0.458 T, & \text{and } T < T_g \\ 1050.97 - 0.628 T, & \text{and } T \geq T_g \end{cases} \quad (3.12)$$

where T_g is the glass transition temperature of ABS.

The polymers are made of long chains having branches and cross links which result in complex structures. Even in molten stage, they tend to retain the cross links. This linkage ultimately contributes to the elastic behaviour of polymers. When the polymer is subjected to shear, these links tend to break. Hence polymers in two adjacent layers of flow no longer

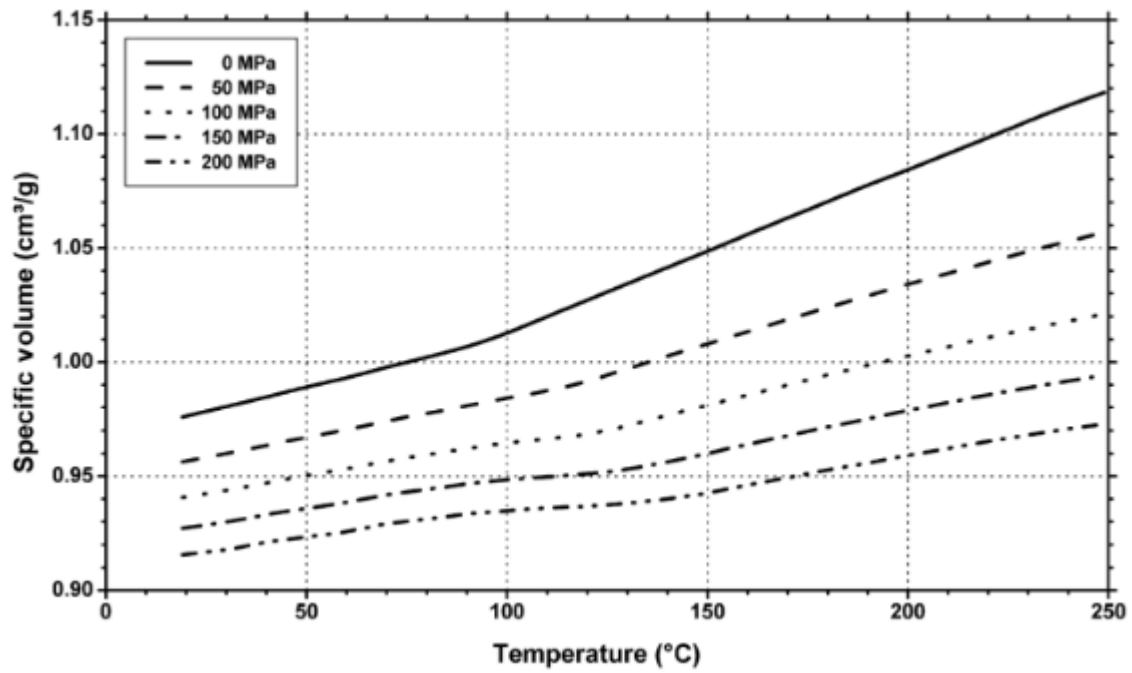


Fig. 3.2 Specific volume vs Temperature for ABS resin [23]

have bonding between them. This reduces the viscosity of polymer melts. Such behaviour is called shear thinning.

ABS melt flows are highly viscous in nature. They exhibit strong non-Newtonian shear thinning effects and are very difficult to compute numerically using the partial differential equations. Instead of that the experimental models which predict the behaviour close to the actual behaviour of the melt can be used. In the present study, a Cross WLF model is used to predict the effect of the shear rate and temperature on the viscosity of ABS through a user defined subroutine.

Cross [24] experimentally found out the relation between shear rate and the viscosity. Hieber and Chiang [25] used a Cross-WLF model for the viscosity of ABS as a function of temperature and shear rate. The cross model relates the viscosity as a function of zero shear viscosity (μ_0) and shear rate ($\dot{\gamma}$) as

$$\mu = \frac{\mu_0}{1 + \left(\frac{\dot{\gamma}\mu_0}{\tau}\right)^{(1-n)}} \quad (3.13)$$

The effect of temperature on the viscosity is incorporated using a WLF function which relates the zero shear viscosity with temperature. The WLF model is given as

$$\mu_0 = \begin{cases} E e^{\left(\frac{-A_1(T-T_g)}{A_2+(T-T_g)}\right)}, & T > T_g \\ E, & \text{and } T < T_g \end{cases} \quad (3.14)$$

In the above equations, τ , n , E , A_1 and A_2 are the material constants which are found out experimentally. For ABS the values of these constants are given in table 3.2

Constant	Value	Unit
τ	2.9×10^4	Pa
n	0.33	-
E	3.63×10^{11}	Pa-s
A_1	27.21	-
A_2	92.85	K

Table 3.2 The values of Cross WLF viscosity model parameters for ABS

The value of viscosity predicted by the Cross WLF model approaches to E which is typically a very high value as the temperature of the melt approaches to the glass transition temperature. It implies that the fluidity of polymer melt reduces as it approaches the glass transition temperature.

In the current solver, the Cross WLF model is coupled as a user defined function as given in the following sub-section.

3.6.1 User defined function for Cross WLF model

```
#include "udf.h"

DEFINE_PROPERTY(ps_viscosity, cell, thread)

{

    real mu;

    real mu0;

    real temp = C_T(cell, thread);

    real gammadot = C_STRAIN_RATE_MAG(cell, thread);

    if (temp > 373.)
    {

        mu0 = 3.63e11*pow(10.0,11.0)*exp(-(27.21*(temp-373.0))/(92.85+(temp-373.0)));

    }

    else

    {

        mu0 = 3.63e11*pow(10.0,11.0);

    }

    mu = mu0/(1.0+pow((mu0*gammadot/29000.0),0.67));

    return mu;

}
```

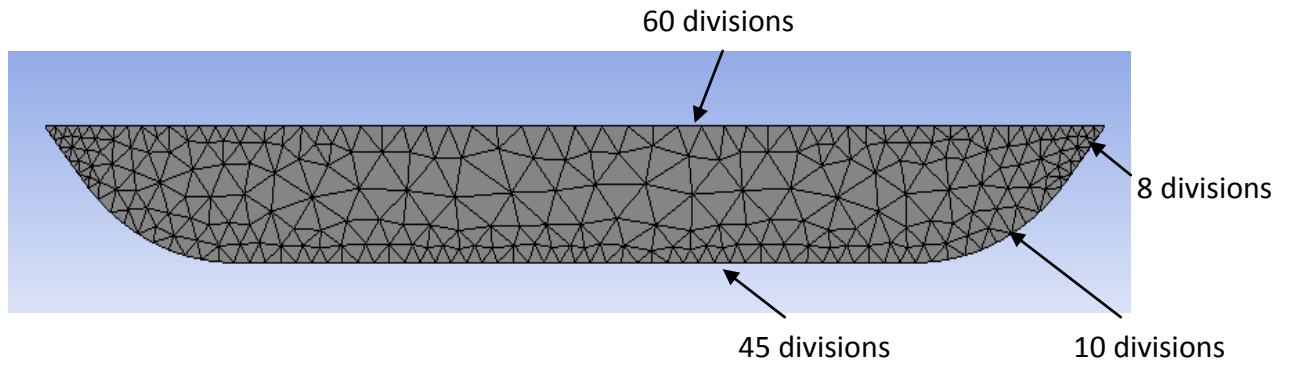


Fig. 3.3 Tetrahedral mesh applied on the flow channel

3.7 Mesh generation

The flow channel is a long tapered channel with cross section similar to the trapezoid. A collocated tetrahedral mesh is used as shown in fig. 3.3.

The drag flow in the flow channel takes place due to the motion of the screw with respect to the barrel. At the corners of the channel, the barrel wall is stationary and screw wall is in motion. Due to the no sticking condition, the fluid adjacent to the barrel wall remains stationary while the fluid near the screw wall moves with the barrel velocity creating large velocity gradients. These gradients result in high shear stresses and thus high viscous heating. High viscous heating supports the melting process in the melt section. Due to high shear thinning the viscosity of the fluid decreases. In order to accurately model these effects, a fine mesh is needed near the corners. Also the melt film generates near the barrel wall. As the mesh near the barrel wall is made finer, the effect of melt film is captured with improved accuracy. Hence a mesh shown in fig. 3.3 is used for analysis.

No. of elements: 258214

No. of nodes: 431237

As shown in fig. 3.3, the inclined screw wall, the fillet and the bottom screw wall are uniformly divided into 8, 10 and 45 divisions respectively. The barrel wall is divided into 60 elements with bias factor of 10. The divisions are biased and made finer towards the corner of the geometry. The bias factor is selected on the basis of the gradients generated at the corner.

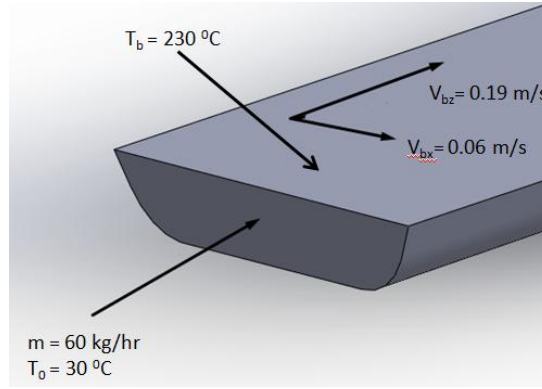


Fig. 3.4 Relative motion between screw and barrel and the boundary conditions

3.8 Boundary conditions

In this method, the screw is considered fixed and the barrel is considered to be rotating with a constant speed (N) as shown in fig. 3.3. The tangential velocity of barrel is given as

$$V_b = \pi D N$$

The screw channel is inclined to the barrel axis at angle θ_h . Hence the tangential velocity of barrel is at an angle θ_h to the flow direction. The down channel and cross channel components of barrel velocity are given as

$$V_{bz} = V_b \cos \theta_h$$

$$V_{bx} = V_b \sin \theta_h$$

The barrel wall has a Dirichlet boundary condition as $T = T_b$

No slip and no penetration boundary conditions are applied on both barrel and screw walls. The screw walls are considered adiabatic [26]. For the adiabatic walls, the Neumann boundary condition is applied as

$$\frac{dT}{dn} = 0$$

where n denotes the normal direction to the wall surface

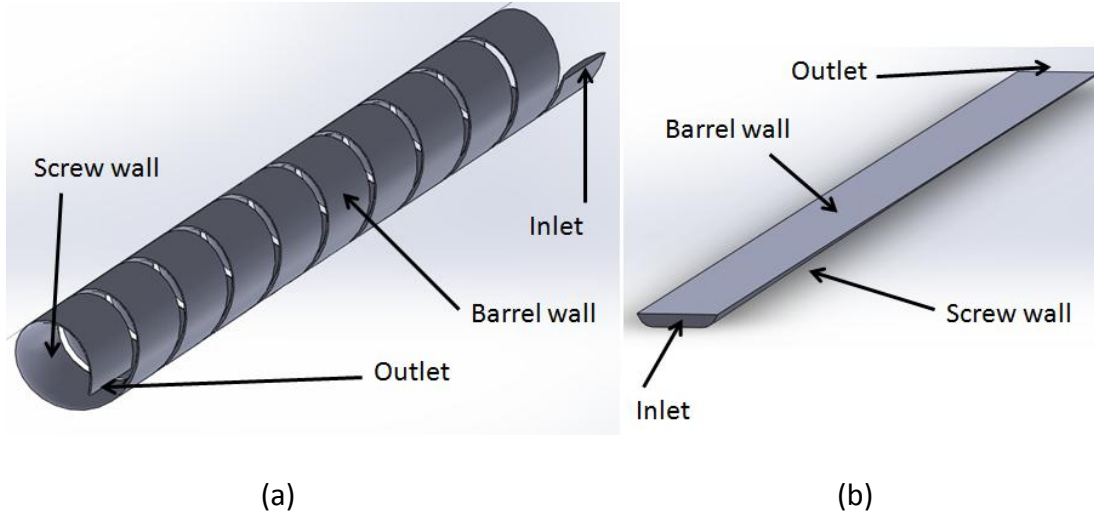


Fig. 3.5 Boundary conditions in (a) wounded and (b) unwounded helical channels

Mass flow rate and polymer temperature is specified at inlet as a boundary condition. The extruder has to compress the polymer so that it overcomes the pressure difference across the nozzle. However for such type of problems, the outlet pressure need not be specified as a boundary condition but it is obtained as a solution.

For mesh generation and model validation (chapter 4), following boundary conditions are used.

Inlet temperature, $T_0 = 30^\circ\text{C}$

Inlet mass flow rate, $\dot{m} = 60 \text{ kg/hr.}$

Screw speed, $N = 60 \text{ rpm.}$

Barrel wall velocities, $V_{bz} = 0.19 \text{ m/s}$

$$V_{bx} = 0.06 \text{ m/s}$$

Barrel temperature, $T_b = 230^\circ\text{C.}$

Parametric study is done by varying the numerical values of boundary conditions to study the effect of process parameters on the quality of polymer coming out of the extruder. The bulk mean temperature of the polymer is calculated to compare the results as

$$T_{bm} = \frac{1}{\bar{w}A_c} \iint_{A_c} wT dA_c$$

where w is the flow velocity along the channel and \bar{w} is the average flow velocity along the channel. A_c is the cross sectional area of the channel.

3.9 Solution method:

The governing differential equations are in elliptic-parabolic form. These equations are highly nonlinear in nature. These equations are similar to the convection diffusion equations. If the central difference scheme is used to discretize these equations, the convection term tends to the unrealistic solutions [22]. Also due to high Peclet number, such solutions can lead to oscillations [16]. To get the correct solutions, an upwind scheme is used. The upwind scheme discretizes the equations in the direction of the convection eliminating the error due to the central difference discretization. In the present study, second order upwind scheme is used to discretize the momentum and energy equations.

Patankar [22] has formulated a Semi Implicit Method for Pressure Linked Equations (SIMPLE) to solve the compressible and incompressible convection diffusion equations. In this study the SIMPLE algorithm is used to solve the governing equations. SIMPLE algorithm implements a pressure correction in order to get the pressure at the cell centres. First step is to assume a pressure field. From the assumed pressure field, momentum equations are solved to get u_0 , v_0 and w_0 . The values of u_0 , v_0 and w_0 are used to solve the continuity equations. Since they are calculated from the assumed pressure values, they need not satisfy the continuity. To satisfy the continuity, corrected factors u^* , v^* and w^* are added and correct values of u , v and w are obtained. Again using these values the momentum and energy equations are solved to get pressure and temperature.

The solution for energy equation was found oscillating. The oscillations were nullified by reducing the underrelaxation factor for temperature. The convergence criteria were set on the residuals for continuity, momentum and energy. The residual of 10^{-3} was set for convergence. The results of the analysis are given in chapter 4.

CHAPTER 4

RESULTS AND DISCUSSION

The three dimensional numerical analysis of the melting process is done by solving the pressure based Navier Stokes equations along with continuity and energy equations coupled with the constitutive model for multiphase compressible non Newtonian flow taking place inside the channel in the Archimedean screw of the single screw extruder. The unstructured tetrahedral mesh is applied and a finite volume based method is used. A second order upwinding scheme is used for discretization. The SIMPLEC algorithm with under relaxation is used to solve the numerical equations. Boundary conditions are varied for the parametric study. The results of the numerical study are presented in this chapter. The chapter consists of the mesh convergence, model validation and parametric study.

4.1 Mesh convergence

The numerical model was tested on three meshes to check the mesh convergence. The meshing was done as stated in chapter 3. Tetrahedral meshes were created by varying the edge sizing. While creating a finer mesh from a coarser mesh, it was made sure that the cell centres in the coarser mesh are retained in the finer mesh. New cell centres were created between two existing cell centres and mesh was made finer. The coarse mesh was refined twice to get two more meshes. The meshes are called as 0.5x mesh, 1x mesh and 2x mesh in this chapter.

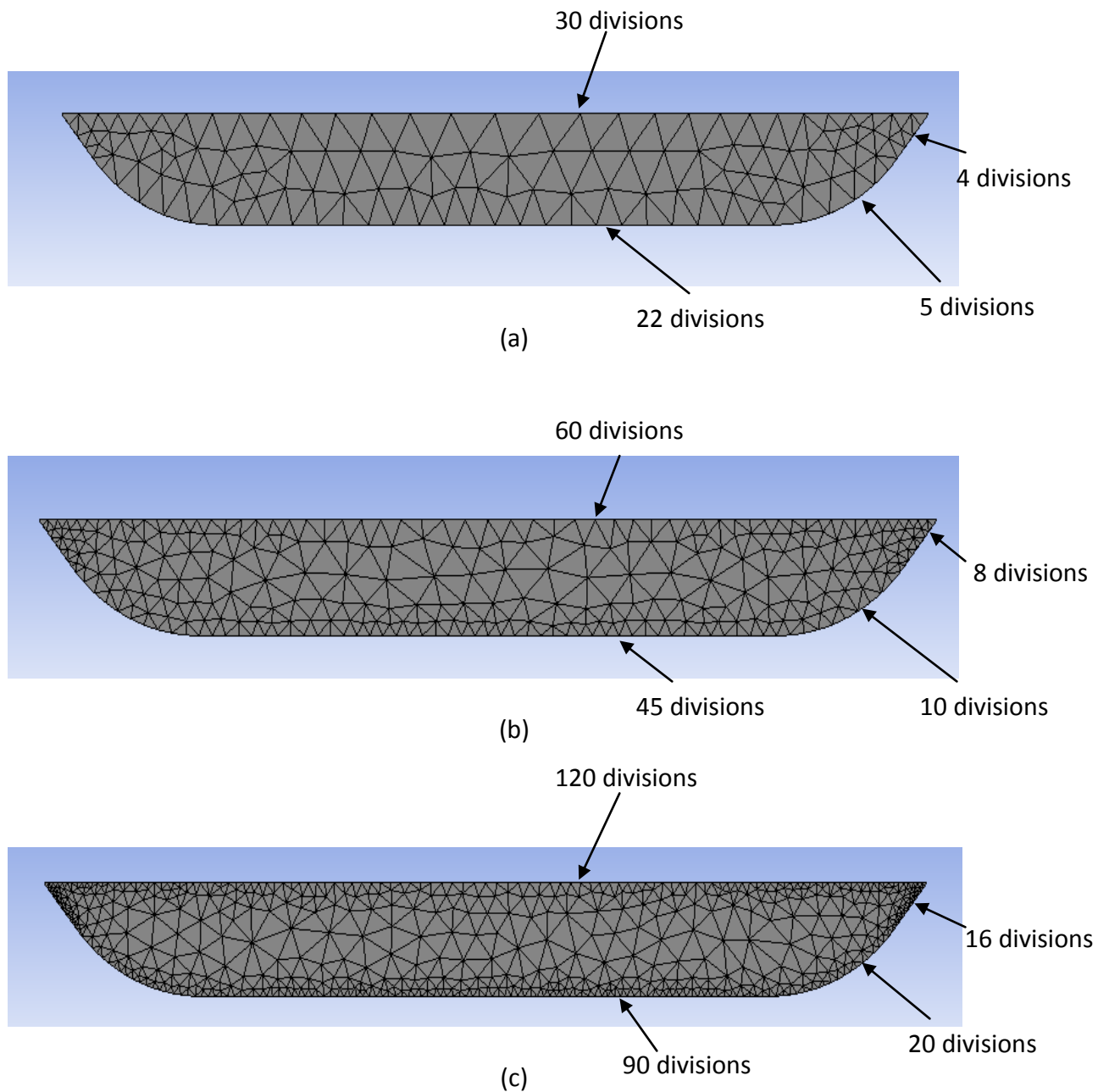


Fig. 4.1 Meshes used for convergence study - (a) 0.5X mesh, (b) 1X mesh, (c) 2X mesh

Fig. 4.1 shows the meshes used for the mesh convergence study. Table 4.1 gives the mesh details. All three meshes were tested with the same boundary conditions and results were obtained. Time required for convergence was also recorded.

Parameter	Mesh 0.5X	Mesh 1X	Mesh 2X
No. of elements	114895	258214	557285
No. of nodes	210103	431237	863348
Convergence	No	Yes	Yes
Convergence time	-	Approx. 81 hrs	Approx 156 hours

Table 4.1 Mesh comparison

All three meshes were tested subjected to the boundary conditions mentioned below.

Boundary conditions:

Inlet mass flow rate = 60 kg/hr.

Inlet solid temperature = 30⁰C

Barrel temperature = 230⁰C

Screw - Adiabatic

Screw speed = 60 rpm.

No slip condition applied on both barrel and screw.

The convergence criteria were selected as the residual values for temperature, velocity and pressure. The solution was said to be converged when the residuals were found below 0.001 for velocity and pressure and 1×10^{-6} for temperature.

In the present problem, the velocity gradients of the polymer near the screw clearance are very high. Due to the high velocity gradient, shear rate is high which results in the viscous heating of the polymer. Melting of the polymer first initiates in this region. Hence the temperature gradients in that region are very high. While solving the discretized governing equations, high gradients can pose a difficulty in convergence as the residual for every iteration is large. Hence to avoid the large residuals, a fine mesh is needed to in the

area of high gradients. The mesh 0.5X was found insufficiently fine in that region and the solution using 0.5X mesh could not converge due to the same.

The solution was converged when meshes 1X and 2X were used. However the time required to converge the solution was almost double in case of the 2X mesh than that of the 1X mesh. The comparison of melt profile is shown in fig. 4.2. For both the meshes, solid bed profile, melt temperature and solid bed percentage was compared. In fig. 4.2, the melt profiles are compared at various normalized axial lengths. Axial length is stated in terms of diameters, i.e. axial length of 5 equals to 5 times the diameter. From fig. 4.2 it can be observed that the 2X mesh predicts the melting with better accuracy. From fig. 4.1, it is clearly seen that the 2X mesh is finer than the 1X mesh near the barrel wall. The melt film is generated near the barrel wall first. Therefore high temperature gradients are present near the barrel wall. Due to finer mesh, the temperature gradients are captured more accurately when 2X mesh is used for simulations as shown in fig. 4.2. A very little difference in overall solid bed profile is observed when both the meshes are compared.

Temperature profiles were also studied for both 1X and 2X meshes and the results are shown in fig. 4.3. Similar to the melt fraction, temperature profiles show that the mesh 2X captures the temperature at the barrel surface more accurately than the mesh 1X.

Fraction of solid bed in the metering zone were compared for both the meshes as shown in fig. 4.4. It is clearly seen that the mesh 2X predicts lesser solid bed due to the better calculation of the melt film thickness between the barrel wall and the solid bed. As the melt film thickness increases, the solid bed thickness decreases and hence the fraction of solid decreases. But solid bed fraction in mesh 2X increases along the length as the increased melt film thickness predicts lesser volumetric heating and reduces the melting rate. Thinner melt film predicted in mesh 1X predicts better melting rate and solid fraction prediction comes out to be less than the 2X mesh. However the maximum difference between the two results was found to be 6.2%.

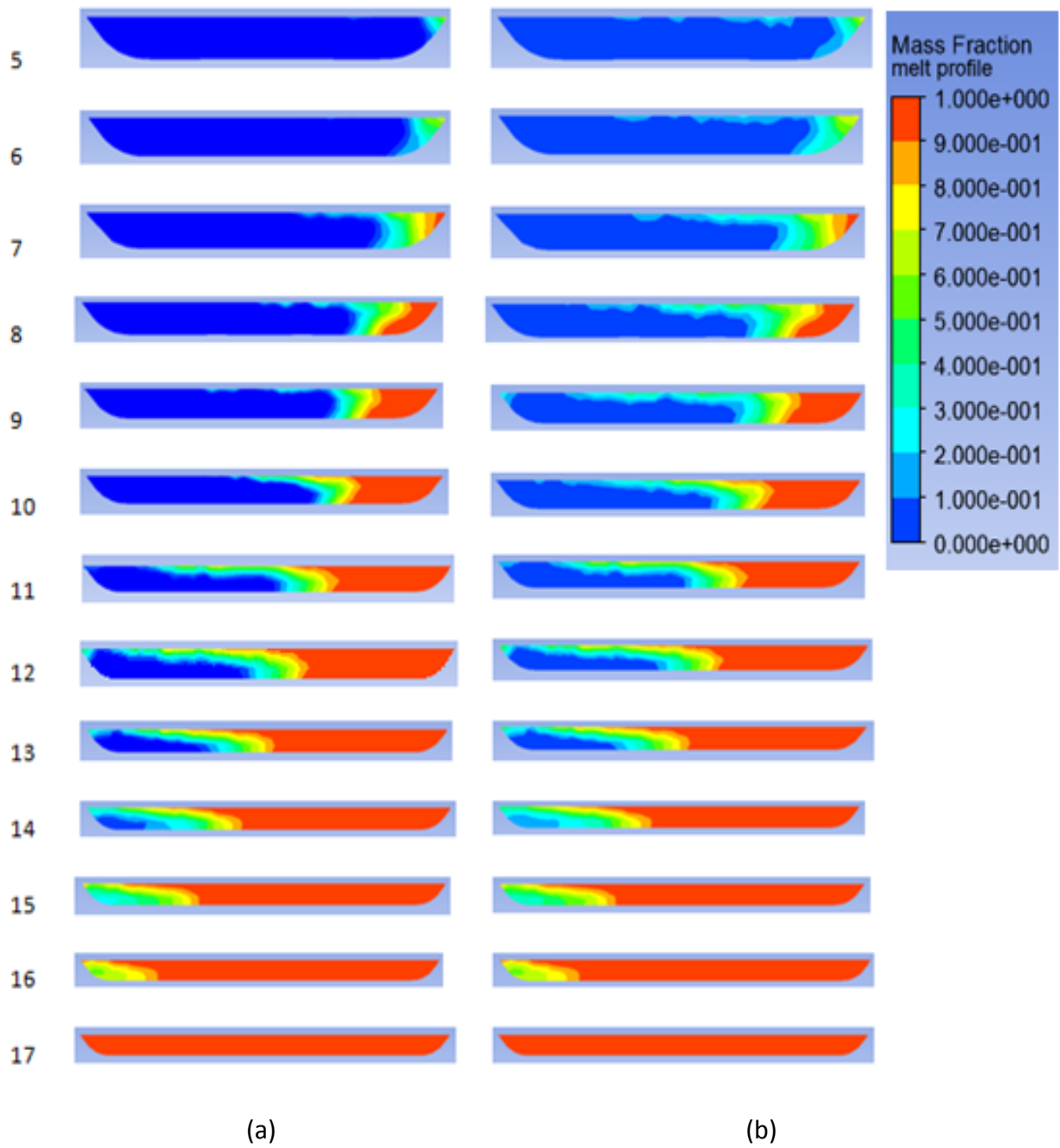


Fig. 4.2 Melt profile at various axial lengths (a) 1X mesh (b) 2X mesh

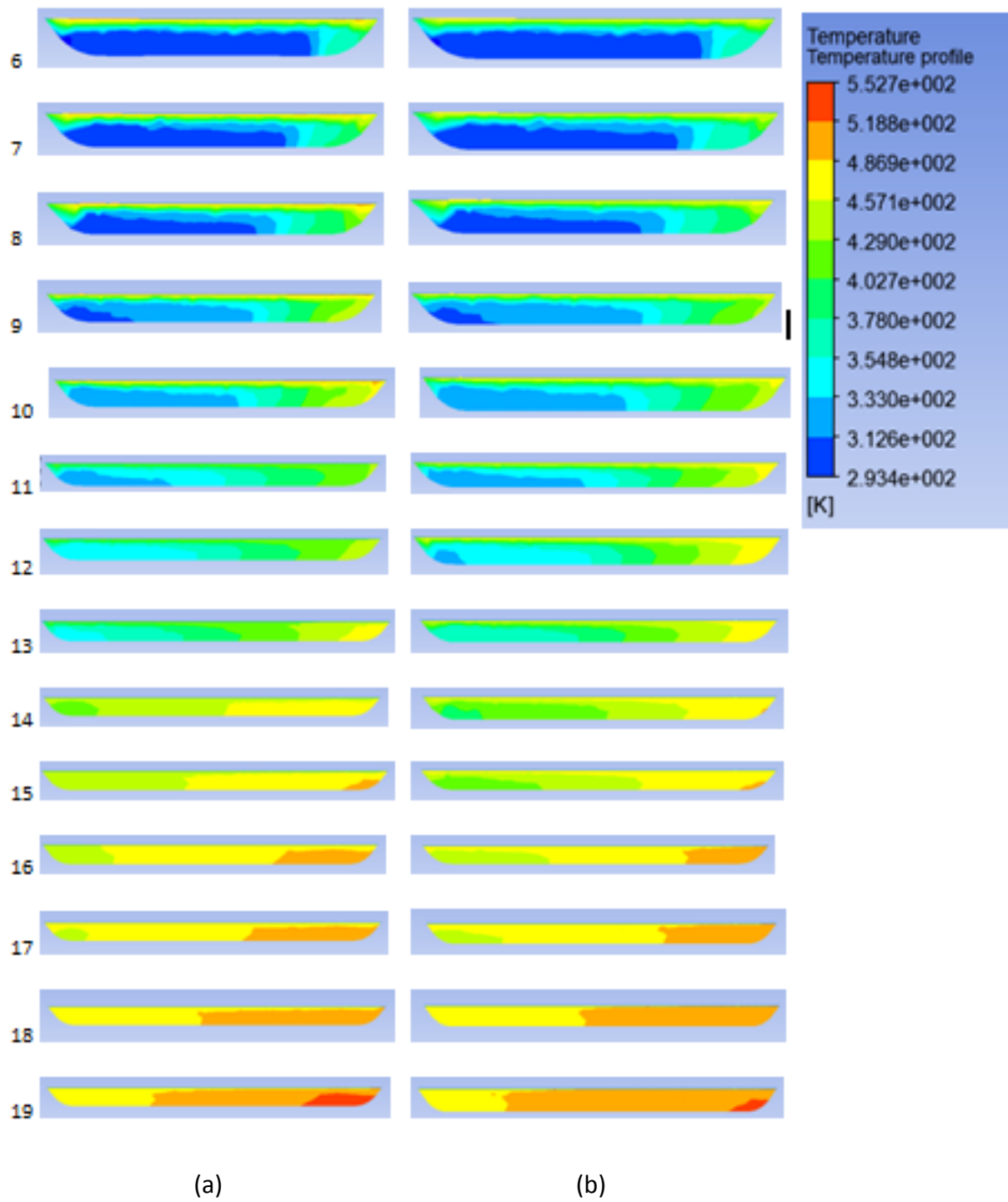


Fig. 4.3 Temperature profile at various axial lengths (a) 1X mesh (b) 2X mesh

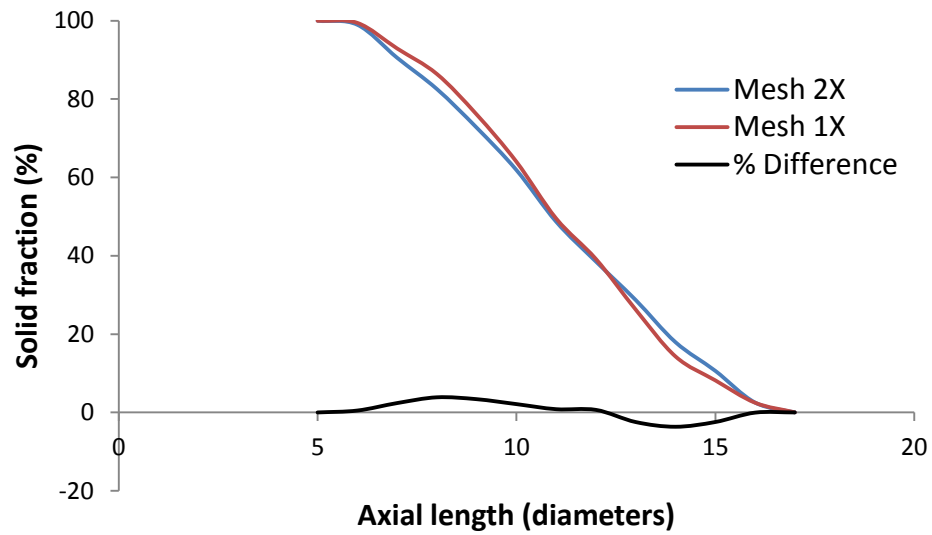


Fig. 4.4 Comparison of solid fractions along the axial length

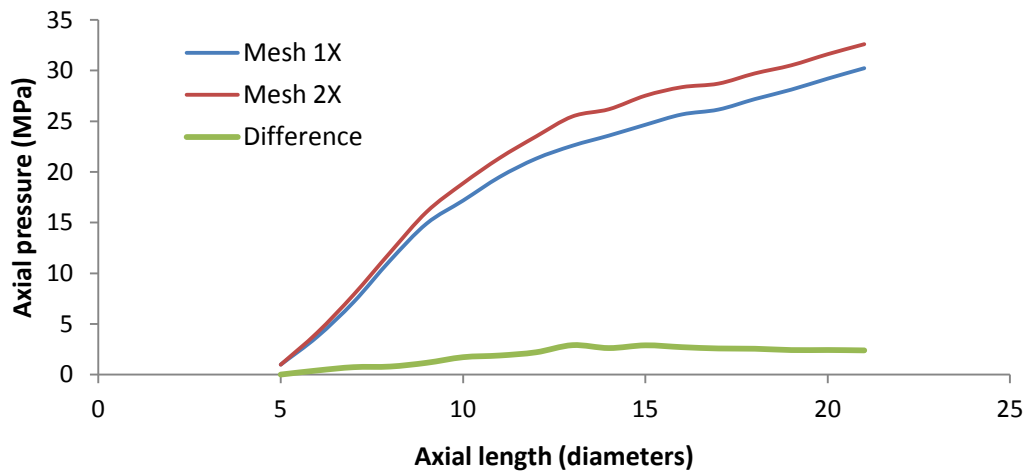


Fig. 4.5 Comparison of axial pressure along the axial length

Variation of axial pressures along the length for both the meshes were compared. It was found that the mesh 2X predicts more axial pressure than mesh 1X. However the difference between the two was found less than 3.5 MPa which is reasonable. Trends of both the results show that the axial pressure increases rapidly in the melting section and increases gradually in the metering section. Rapid increase in melting zone is due to its compressive geometry. As the material flows through the constant depth metering zone it gradually develops the pressure.

In mesh convergence study it was observed that the 2X mesh produces the same results as the 1X mesh. Thus refining the 1X mesh further does not alter the nature of the results. Although refining the mesh predicts more accurate results, the desired accuracy can be obtained by using 1X mesh. Also the computation cost gets almost double as we refine the mesh further. Taking in the account the improvement in the accuracy and increase in the computational cost and time, it was decided to use the 1X mesh for all the numerical simulations performed in the study.

4.2 Model validation

In the past few decades, a lot of experimental work has been carried out to study the melting in the single screw extruder (Maddock [6], Cox et. al.[7], Marshall and Klein [8], Tadmor et. al. [9], Kulas and Thorshaug [10], Mount and Chung [12], Altinkaynak et. al. [17]). However there has been a scarcity of published work in the numerical treatment of the process. Altinkaynak et. al.[17] performed a steady state incompressible multiphase flow analysis on the process. Their results were in good agreement with their experimental data. They performed the screw freezing experiments to observe the melting process using Acrylonitrile Butadiene Styrene (ABS). They used the same process which was developed by Maddock [6]. They operated the screw extruder till the steady state was achieved. Then the screw was stopped and the polymer inside the screw was allowed to solidify by air cooling. A small black pigmented resin was added to the screw which had a lower melting point than the main material. This allowed the black resin to get melted first. After freezing, the black resin identified the molten part while the original white colour illustrated the solid bed profile. The solidified polymer in the screw channel is then peeled off the screw and cut

along the cross section to observe the solid bed profile at that particular cross section. In the present study, the numerical results are compared with the experimental and numerical results reported by Altinkaynak et. al [17].

For current study, a screw of diameter 63.5 mm was selected. The channel width is of 55.5 mm with corner radius of 5 mm. Channel depth in the metering section is 3.18 mm and the compression ratio is 2.8.

4.2.1 Boundary conditios:

Inlet temperature, $T_0 = 30^{\circ}\text{C}$

Inlet mass flow rate, $\dot{m} = 60 \text{ kg/hr.}$

Screw speed, $N = 60 \text{ rpm.}$

Barrel wall velocities, $V_{bz} = 0.19 \text{ m/s}$

$$V_{bx} = 0.06 \text{ m/s}$$

Barrel temperature, $T_b = 230^{\circ}\text{C.}$

Fig. 4.6 shows the comparison between the melting observed in the experiments and the melting predicted by the numerical analysis. Both the experimental and numerical simulations show that the Maddock mechanism is followed during the melting of the polymer. In both the results, a melt film is generated near the barrel wall as the polymer progresses. Due to the motion of the barrel along the cross flow direction drags the polymer present in the melt profile towards the active flight. An accumulation of polymer melt near the active flight forms a melt pool in the region. As the polymer progresses in the channel, the melt pool size increases.

It can be observed in both the results that the solid bed width decreases as the polymer progresses in the screw. It is hence proved that the melt pool present near the active flight supports the melting as stated by the Maddock's mechanism.

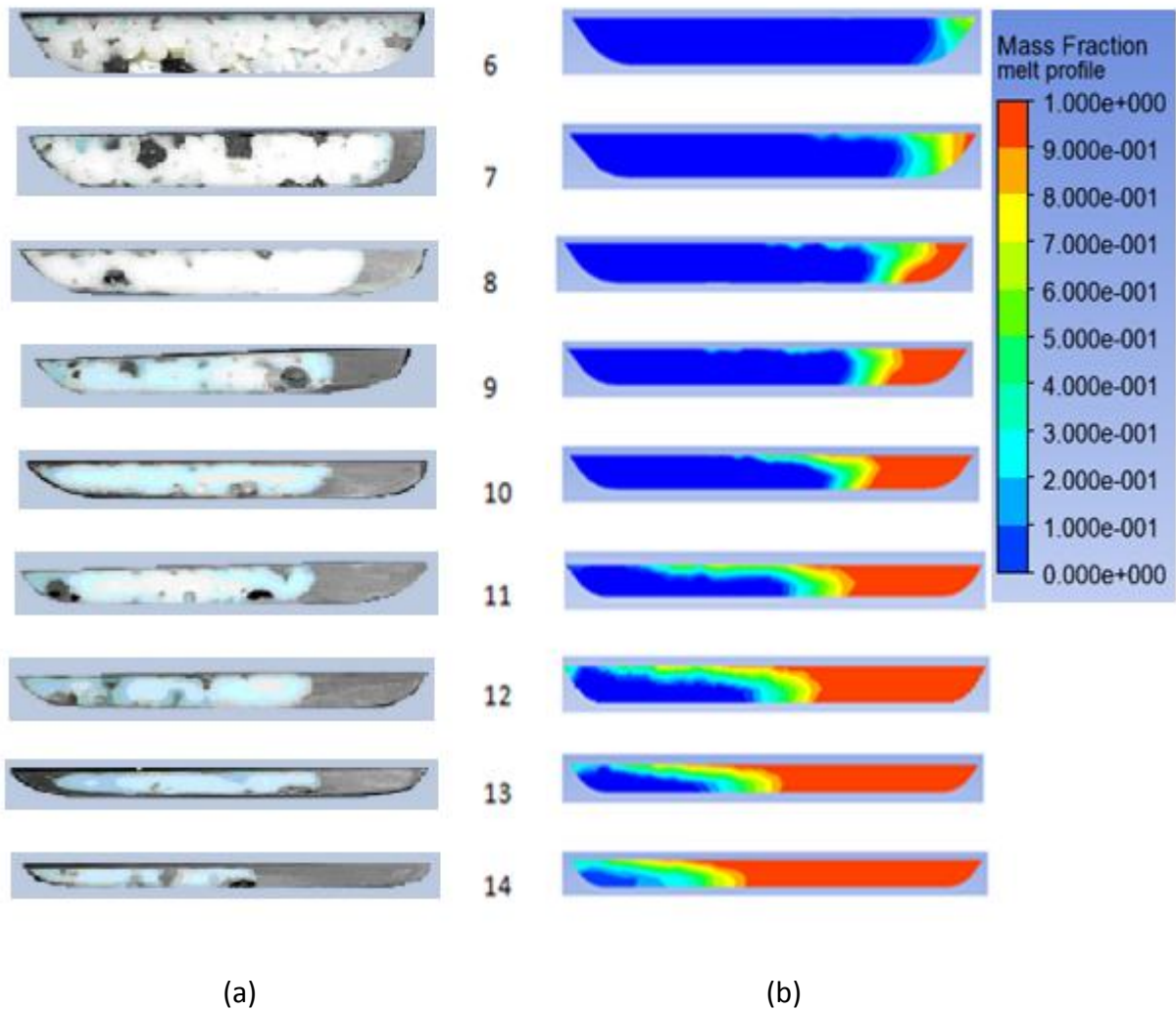


Fig. 4.6 (a) Melt profile observed in experiments (Altinkaynak et. al. [17])

(b) Melt profile predicted by the numerical analysis

Experimental results show a small film of the polymer melt adjacent to the screw wall near the end of the metering zone. Particularly at the length of 12 diameters and onwards the melt film is observed near the screw. The melt film is generated due to the elevated temperature of the screw. In the results of the numerical analysis, no such melt film was observed near the screw as the screw is considered adiabatic. However in practical situations, the temperature of the screw can raise up to melting temperature of the polymer initiating the melting at the screw wall.

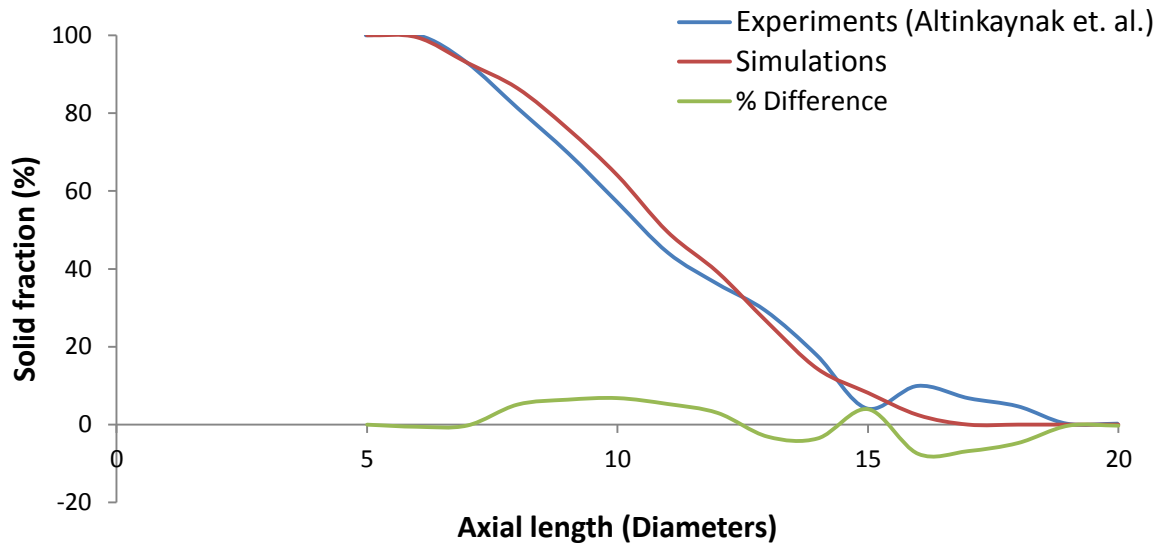


Fig. 4.7 Variation of axial pressure observed in simulations compared with that in experiments by Altinkaynak et. al. [17]

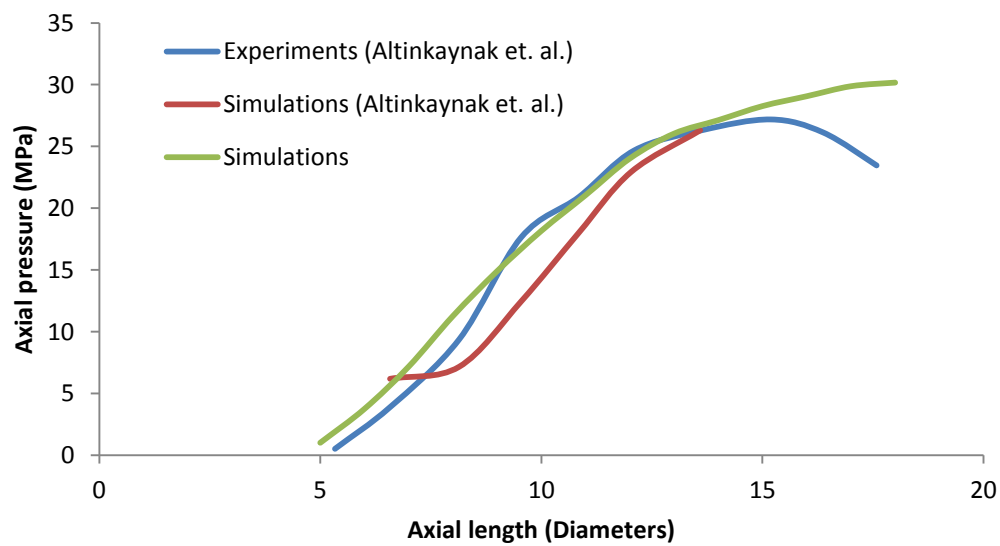


Fig. 4.8 Comparison of the axial pressures predicted by the numerical simulations and the experimental and numerical results reported by Altikaynak et. al.[17]

Comparison between the solid fraction predicted by the numerical analysis and the experimental observations is given in fig. 4.7. The results predicted by the numerical analysis show the trend similar to that observed in the experiments. As the axial length of 6 diameters is crossed, the melting zone of the screw starts and polymer starts melting rapidly. The rate of melting is nearly constant over the entire length of the melting zone. The melting zone ends at the axial length of 14 diameters. At that points experimental data shows a sudden drop in the solid fraction. This could be due to the solid bed breakup. In numerical predictions, no such drop was observed. The melting rate smoothly reduces to zero at the length of 16 diameters. However at the length of 14 diameters, the fraction of solid left was found to be less than 10%. The numerical analysis overpredicts the solid fraction as viscous heating in the clearance is neglected. However the difference between the numerical predictions and experimental observations was observed to be below 7%.

The axial pressure predicted by the numerical model and the recorded axial pressure were compared. The axial pressures predicted in the current study, predicted by the study carried out by Altinkaynak et. al. and the experimentally observed values show the same trend. As the polymer progresses in the channel, the melt pool size increases which raises the pressure in the channel. The comparison is shown in fig. 4.8. Numerical predictions agree with the experimental observations up to the end of the melting zone. In the metering zone, the axial pressure was observed to be decreasing in experiments. However the numerically predicted value of pressure keeps on increasing by a small rate.

The comparison of melt profile, axial pressure and solid fraction shows that the trend captured by the model is correct. However there is a difference between the numerically predicted and experimentally observed data. This error could be due to truncation, fault in the experimental observations, etc. However the current study shows that the modelling is done properly and the same model can be used for parametric study.

4.3 Parametric study

In the melting section of the extruder, the tapered flow channel is heated by the ceramic barrel heaters. Generally the barrel heaters are set to maintain a particular barrel temperature. Due to the heat supplied by the heaters and viscous heating, the polymer melting takes place in the barrel. The melting process is highly influenced by the barrel temperature. To achieve complete melting of polymer, it is essential to set the appropriate barrel temperature. The melting process also depends on the screw speed as it directly influence the viscous heating by varying the velocity gradients developed in the melt film and thus varying the shear rates. Also the flow rate defines the amount of material flowing in the channel per unit time. Mass flow rate of the polymer melt can be a deciding factor in the design process of the extruder screw. Screws are designed to accommodate a particular amount of polymer melt making sure that it melts completely before going in the metering section.

The metering section serves the purpose of homogenizing the polymer melt before it goes to the nozzle. In the metering section, cross channel flow transfers the heat from the heated barrel surface towards the screw root. As the polymer flows along the metering section, the uniformity in the temperature is achieved by the cross channel flow heat convection. The cross channel flow is also affected by the screw speed and the flow rate. Hence studying the effect of barrel temperature, flow rate and screw speed are the determining factors which affect the polymer quality at the exit of the metering section.

In present study, the variation of melt profile, solid fraction, axial pressure and the bulk mean temperature are calculated to compare the polymer quality obtained. The variation in the polymer quality with the variation in the barrel temperature, screw speed and the feed rate are studied.

4.3.1 Variation of barrel temperature

The barrel temperature in extrusion deposition process is always maintained at a constant temperature. In the present study the effect of barrel temperature on the melting process and the end quality of polymer is shown. The study is done by varying the boundary condition of barrel temperature. The barrel temperature is set at 230⁰C, 250⁰C and 270⁰C to study the melting process. For all the simulations, mass flow rate of polymer is constant at 60 kg/hr. The inlet temperature of polymer is 30⁰C and the screw speed is 60 rpm.

Fig. 4.9 shows the variation in the melting with the barrel temperature. The melting takes place due to two heat sources which are the heat coming from the barrel and the heat generated due to viscous dissipation. In fig. 4.9 it can be clearly seen that the melting rate reduces as the barrel temperature increases. As the barrel temperature increases, more melting takes place near the barrel wall. Hence a thicker melt film is generated between the barrel wall and the solid bed. The velocity gradients in thicker film are less than those in the thinner films resulting in lower shear rates. Hence viscous heating is reduced as barrel temperature is increased. Due to reduced viscous heating, polymer melting rate decreases and more axial length is required to complete the melting process.

Fig. 4.10 shows the temperature distribution in the melting and metering sections. In the metering section (diameters 15 and beyond), as the barrel temperature increases, the convective heat transfer takes place increasing the temperature of the whole polymer melt. The heating due to the viscous dissipation further adds the heat to the polymer increasing the temperature of polymer melt beyond the set barrel temperature. Due to cross channel flows, the heat accumulation is found near the active flight and temperature of the region near the active flight was found slightly more than the rest of the channel. In all the cases, a temperature more than the barrel temperature by 15⁰C to 20⁰C was found.

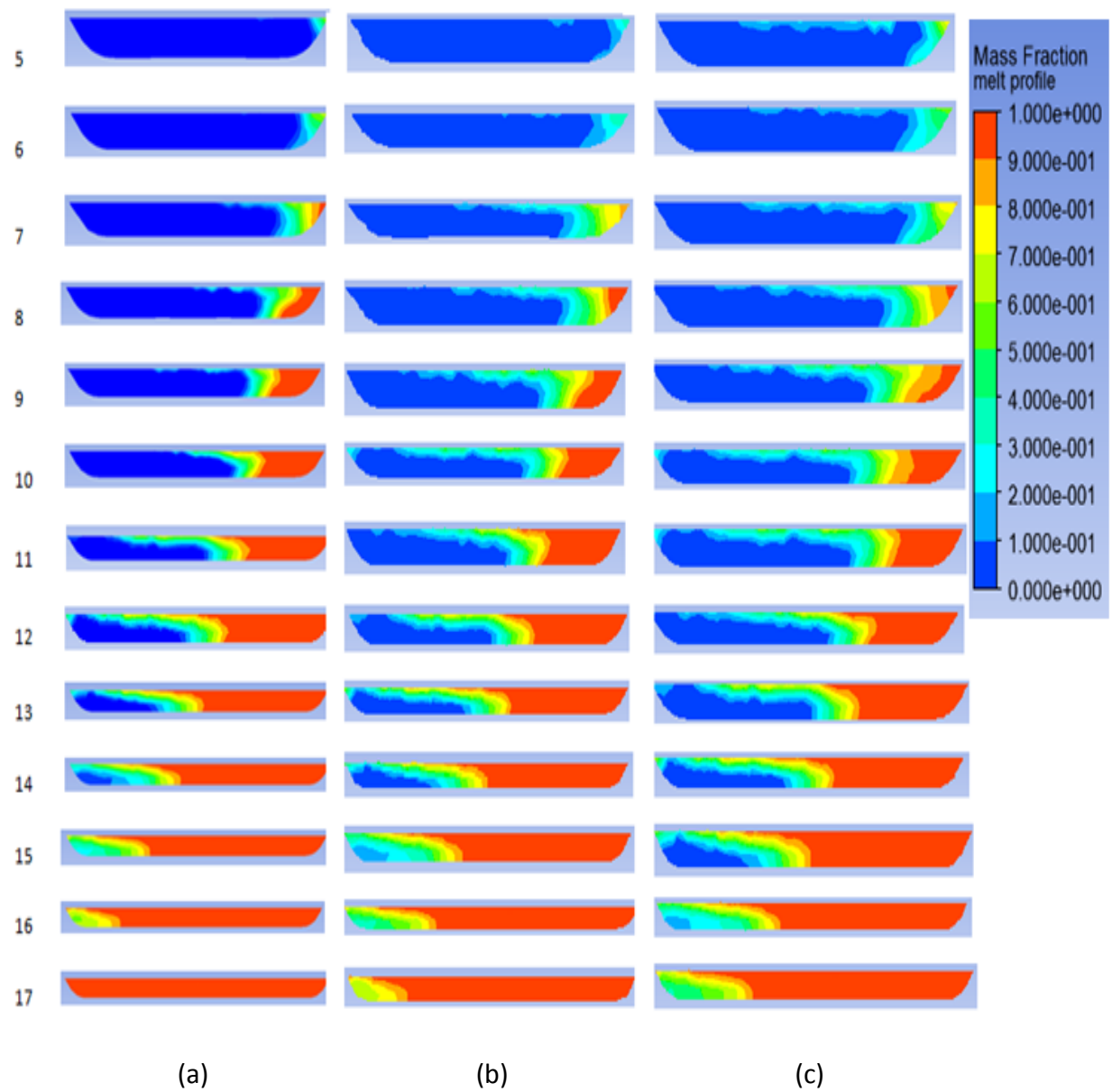


Fig. 4.9 Predicted melting in the melting section of the extruder at the barrel temperature of

(a) 230°C (b) 250°C (c) 270°C

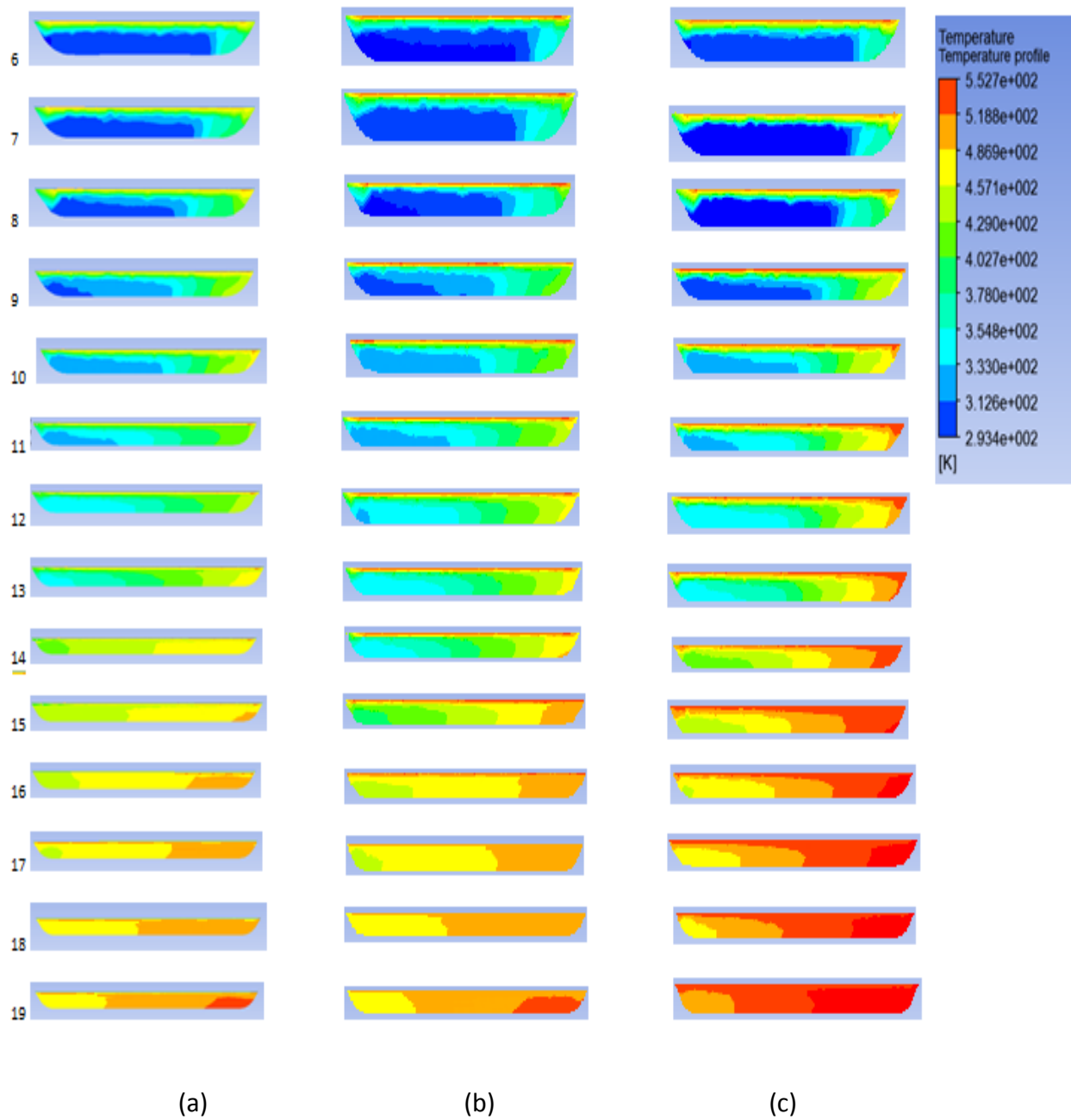


Fig. 4.10 Predicted temperature profiles in the melting section of the extruder
at the barrel temperature of (a) 230°C (b) 250°C (c) 270°C

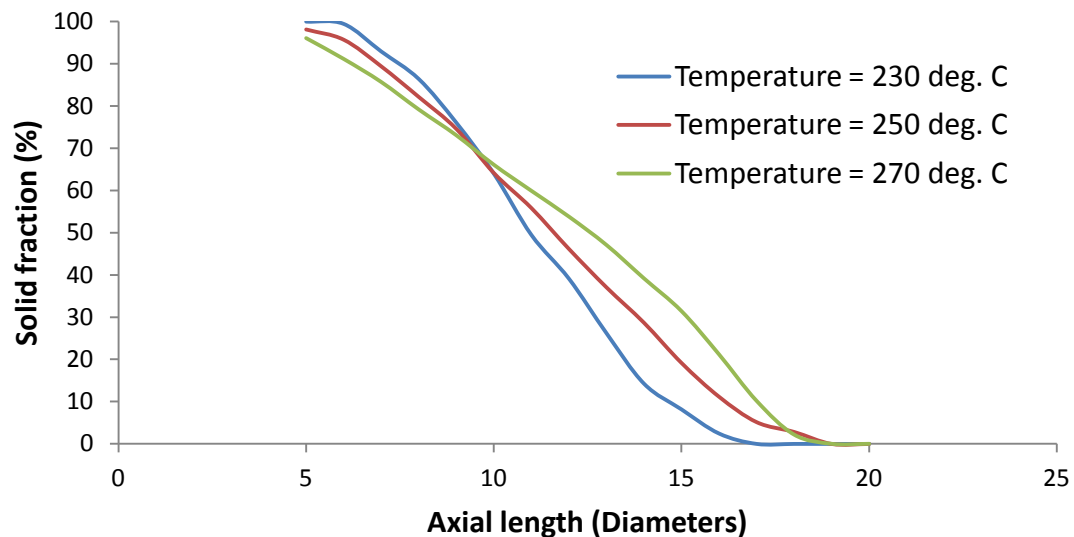


Fig. 4.11 Predicted solid fraction along the axial length in the melting section of the extruder at the barrel temperature of 230⁰C, 250⁰C and 270⁰C

The fig. 4.11 shows the variation of solid fraction as the polymer progresses along the flow channel. As the barrel temperature increases, initial melt film becomes thicker decreasing the solid fraction. The plot shows less solid fraction at the initial stage for increasing temperature. Because of the thickening of the melt film, less viscous heat is produced and melting rate reduces. Hence even with higher barrel temperature, melting process takes more time to complete. For given screw geometry and boundary condition, the melting completes at about 15 diameters at the barrel temperature 230⁰C while it takes 18 diameters at the barrel temperature of 270⁰C.

Sr. No.	Barrel temperature (⁰ C)	Axial pressure (MPa)
1	230	30.17 MPa
2	250	29.93 MPa
3	270	29.51 MPa

Table 4.2 Axial pressure developed at the end of the metering section

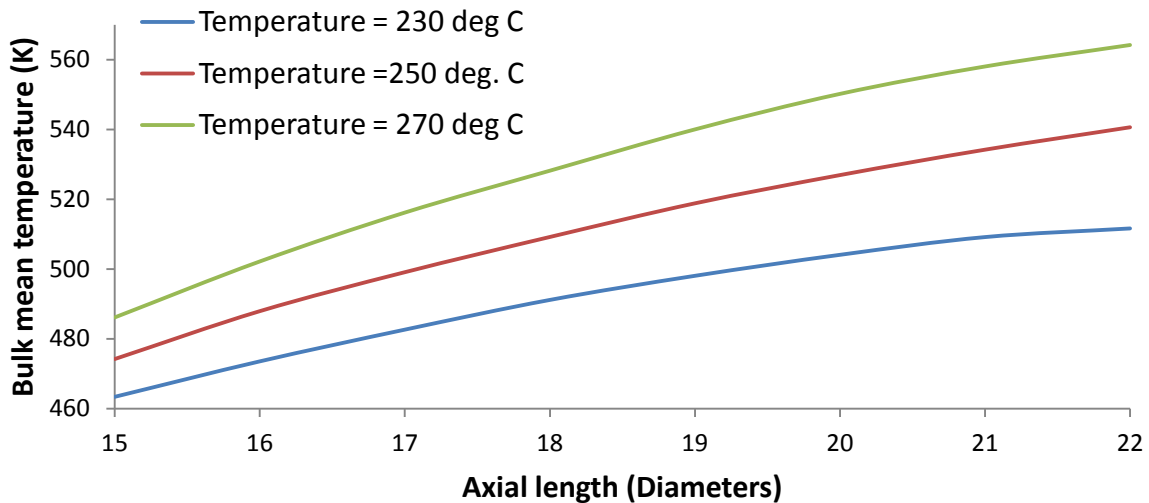


Fig. 4.12 Predicted bulk mean temperature in the metering zone

for barrel temperatures of 230⁰C, 250⁰C and 270⁰C

Table 4.2 shows the axial pressure developed at the end of the metering zone. No significant effect of barrel temperature was observed on the axial pressure developed during the flow through the melting and metering zones of the channel.

Variation of bulk mean temperature with the barrel temperature is shown in fig. 4.12. As the barrel temperature increases, the bulk mean temperature of the polymer melt entering in the metering zone is higher. In the metering zone, the bulk mean temperature increases steadily due to barrel heating and viscous dissipation. As the polymer progresses in the metering zone, the convective heat transfer takes place due to cross channel flow and heat is transferred from the barrel wall to the screw wall till a uniform temperature distribution is reached. It is observed that the temperature at the exit of the metering zone is always higher than the barrel temperature. The additional heat causing this temperature rise is generated by viscous dissipation.

4.3.2 Variation of flow rate

The design of the extruder screw is based on the amount of the polymer it has to carry per unit time. The length of the screw is designed sufficient to ensure the complete melting of the flow before it goes in the metering section. In current study, the effect of flow rate on the melting process is studied. The flow rates of 45 kg/hr, 60 kg/hr and 75 kg/hr are investigated. The other process parameters are kept constant. The barrel temperature is 230°C and the speed is 60 rpm.

Fig. 4.13 shows a comparison between the melting process as the flow rates are varied. At higher flow rates of 75 kg/hr, 60 kg/hr and 45 kg/hr, the melting was completed approximately at the length of 18 diameters, 17 diameters and 15 diameters respectively. As expected, the channel length required for complete melting of the polymer increases as the flow rate increases while the heat supplied per unit length of the channel remains constant. Fig. 4.14 shows that the slope of the curve remains constant for varying flow rates which indicates that the melting rate is constant throughout the length of the melting zone which again proves the prior statement.

In fig. 4.15 pressure developed in the channel shows a significant variation as the flow rate varies. For flow rates of 45 kg/hr, 60 kg/hr and 75 kg/hr, the pressure developed along the entire length of the screw was found to be 37.07 MPa, 30.17 MPa and 25.65 MPa respectively. It is also seen that the majority of the pressure development takes place in the compressive melting zone of the extruder. However a small amount of pressure is developed in the metering zone as well.

The bulk mean temperature of the melt with less mass flow rate was found more than the barrel temperature by 17°C. Less flow rate results in slower flow having better viscous dissipation. Hence more heat is generated and temperature is raised above the barrel temperature. For higher flow rate, even though the convective heat transfer is better, the viscous heat generation is low which results in less bulk mean temperature.

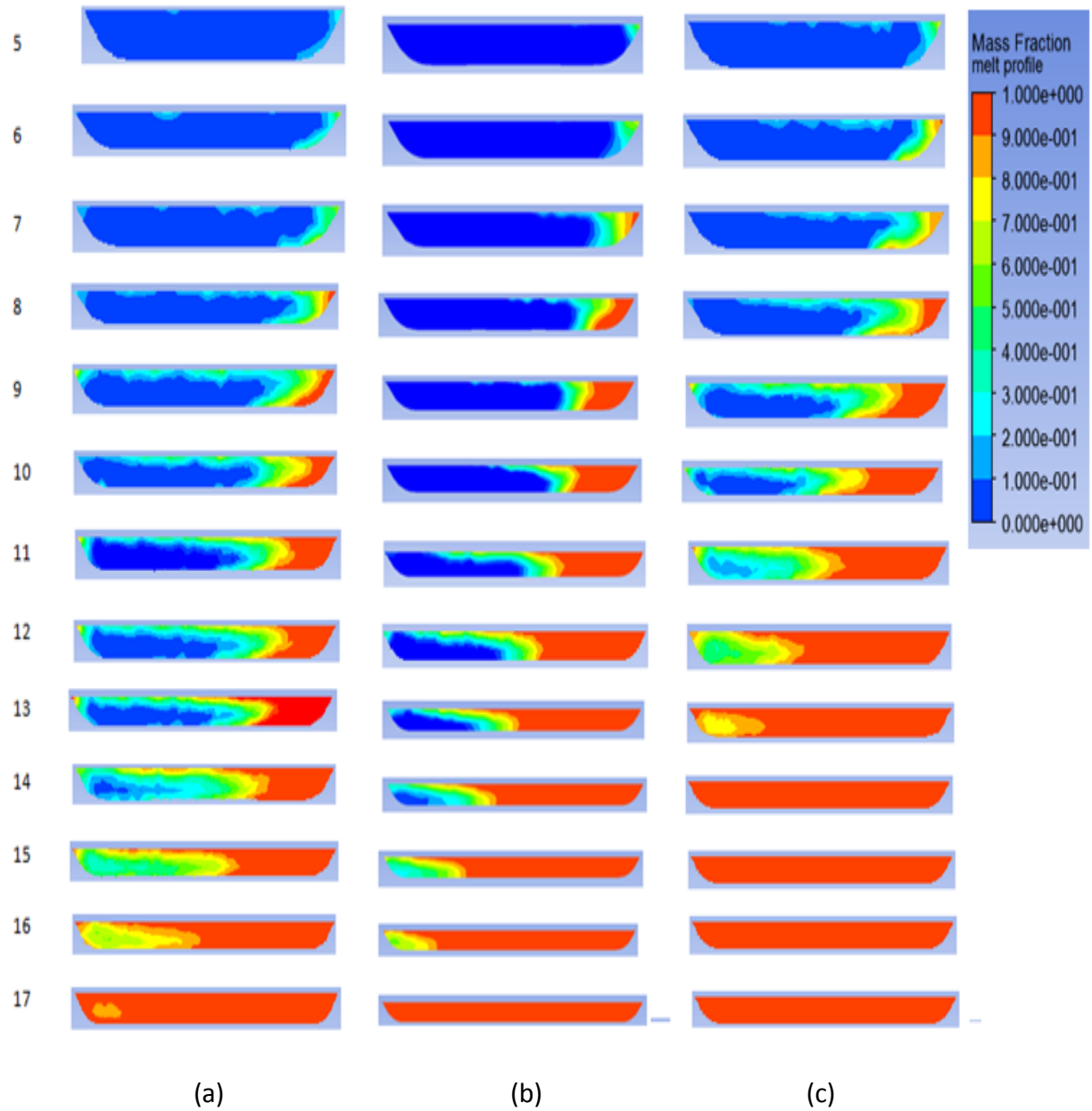


Fig. 4.13 Comparison of melt profiles at various flow rates

(a) 75 kg/hr (b) 60 kg/hr (c) 45 kg/hr

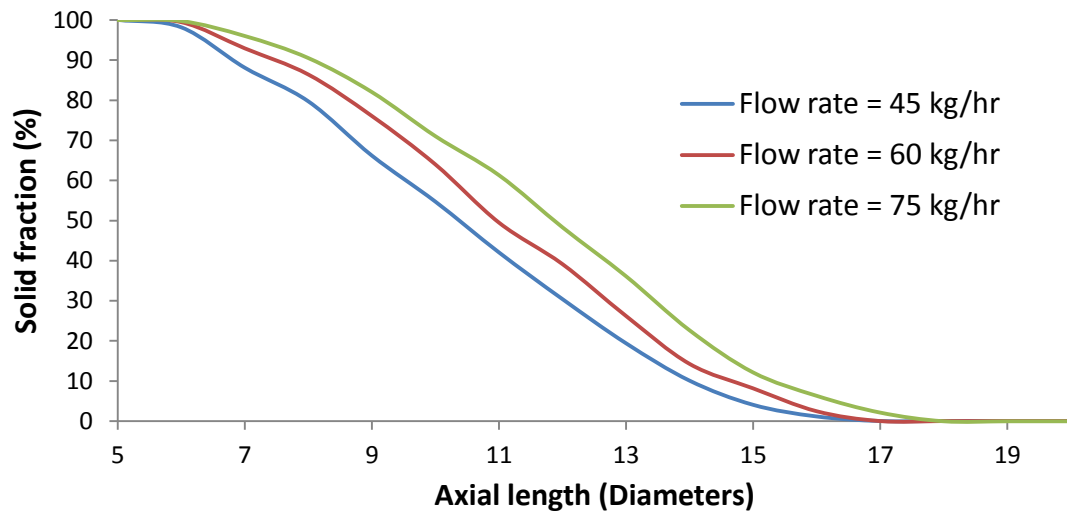


Fig. 4.14 Predicted solid fraction along the axial length for flow rates of 45 kg/hr, 60 kg/hr and 75 kg/hr

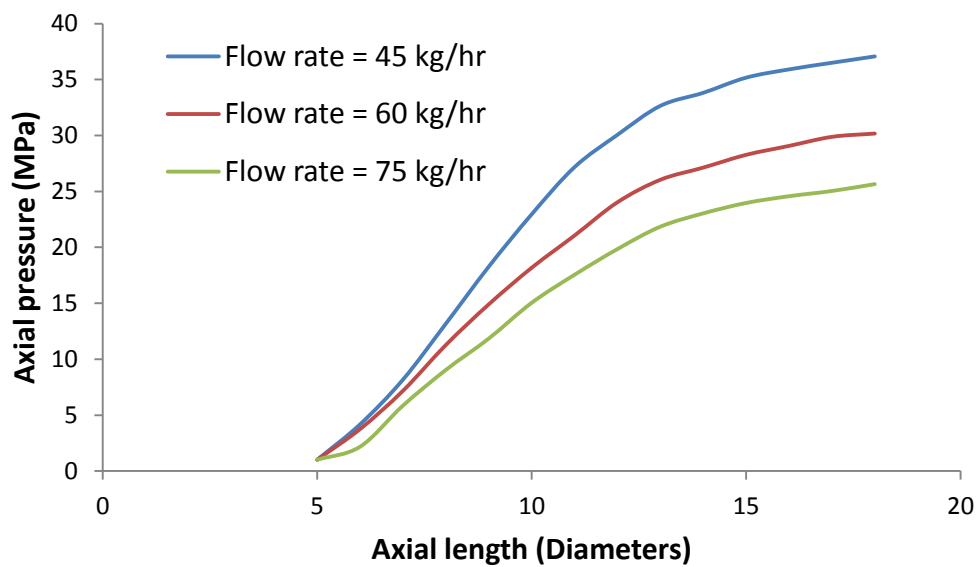


Fig. 4.15 Variation of axial pressure developed along the axial length of flow channel

4.3.3 Variation of screw speed

The screw speed is another important parameter that directly affects the melting and homogenization process in the extruder screw. In the current model it is assumed that the screw is stationary and the barrel rotates around the screw in opposite sense resulting in the same relative motion as in the actual process. Here the barrel speed is varied as 45 rpm, 60 rpm and 75 rpm by changing corresponding barrel velocity and its components along the flow channel and across the flow channel. The remaining boundary conditions are kept constant. The barrel temperature is 230°C and the flow rate at the inlet is 60 kg/hr at 30°C.

During the initial phase of melting, a melt film is generated between the barrel wall and the solid bed. The shear rates in the melt film determine the amount of viscous heating taking place in the film. For higher screw speed, higher shear rates are developed which result in generating more viscous heat. Hence faster the screw speed, faster is the melting rate. In this study the effect of screw speed on melting rate, axial pressure and the bulk mean temperature in the metering zone is studied. Fig. 4.16 shows the melt fraction along the length of the melting zone. For a feed rate of 45 rpm, the melting process is slow due to the low shear rates generating low viscous heat. At the speed of 75 rpm, the melting process is slower in the beginning. The reason behind this could be the time required to generate the initial melt film is higher in this case. As the process progresses the flow rate rapidly increases and the melting is completed at the length of 15 diameters. For 60 rpm and 45 rpm the melting completes at 16 and 17 diameters respectively. Fig. 4.17 shows the comparison of solid fraction for various screw speeds. Melting rate increases with the screw speed due to the reasons stated above.

Variation of axial pressure along the screw channel is shown for various screw speeds in fig. 4.18. As the screw speed increases, an expected increase is observed in axial pressure. As the screw speed is increased from 45 rpm to 60 rpm, the pressure rises from 28.58 MPa to 30.17 MPa. It further increases by 2.4 MPa as the screw speed increases to 75 rpm. Bulk mean temperature slightly increases with screw speed due to better cross channel convection as shown in fig. 4.19.

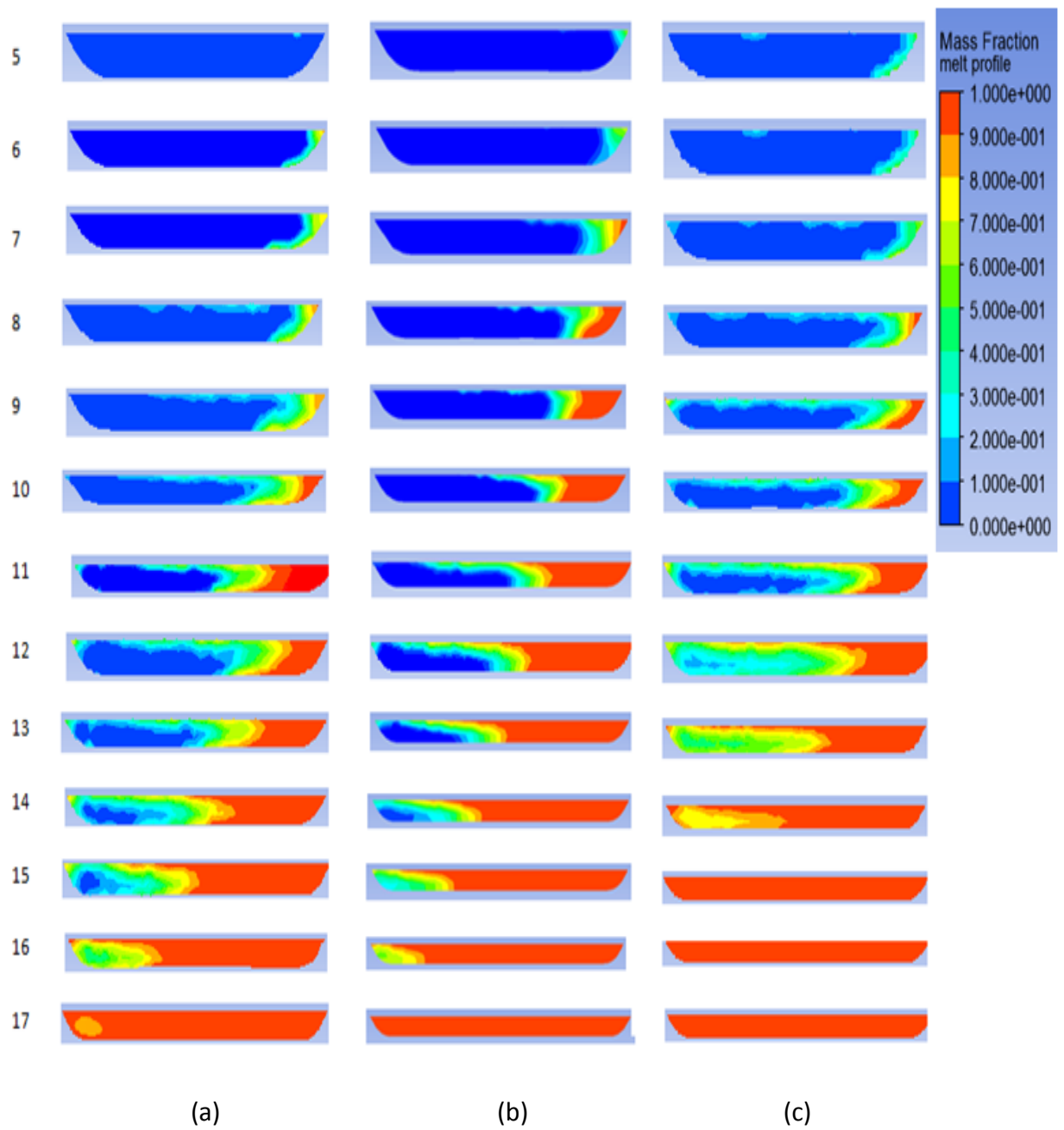


Fig. 4.16 Comparison of melt profiles at various flow rates

(a) 45 rpm (b) 60 rpm (c) 45 rpm

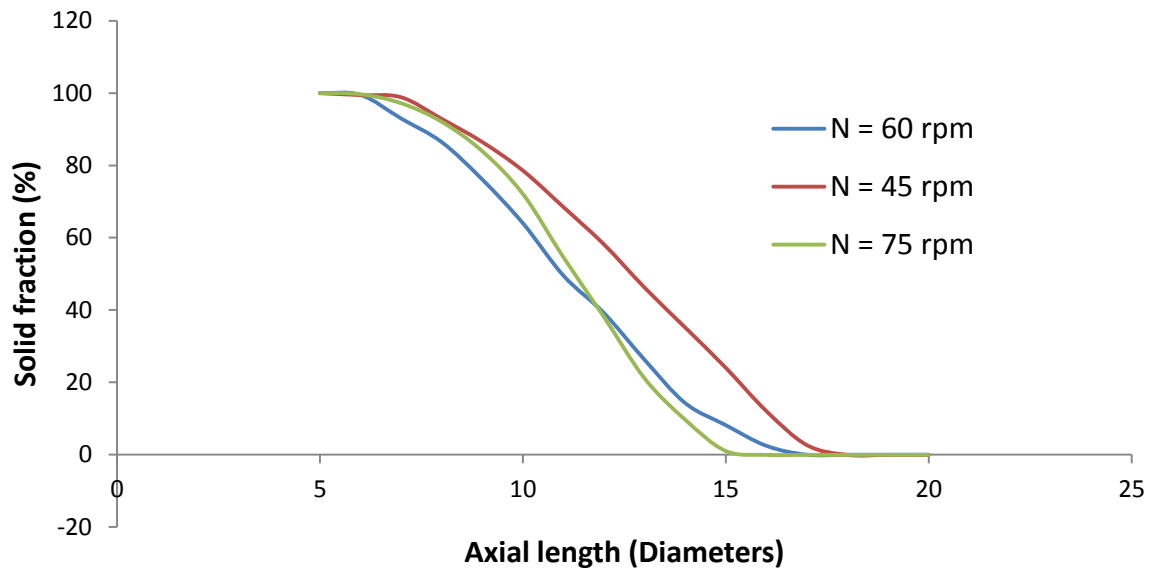


Fig.4.17 Variation of solid fraction along the length of melting zone for various screw speeds

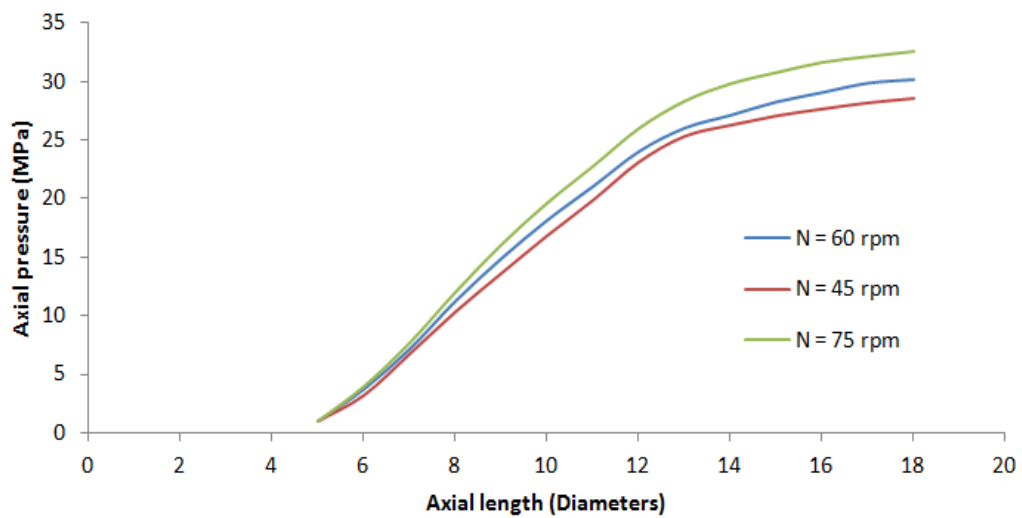


Fig. 4.18 Variation of axial pressure along the axial length for various screw speeds

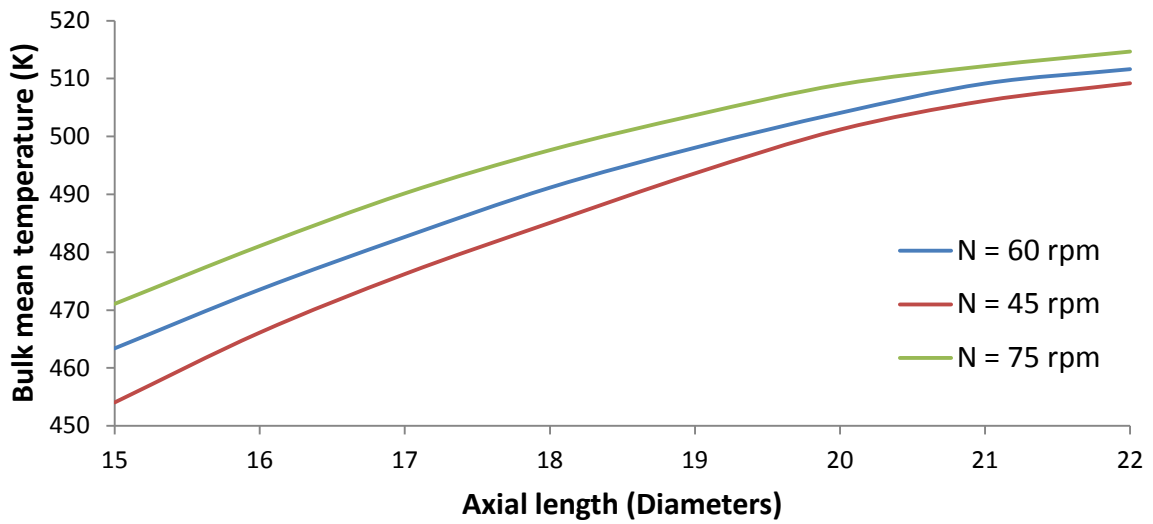


Fig. 4.19 Variation of bulk mean temperature in the metering zone for various screw speeds

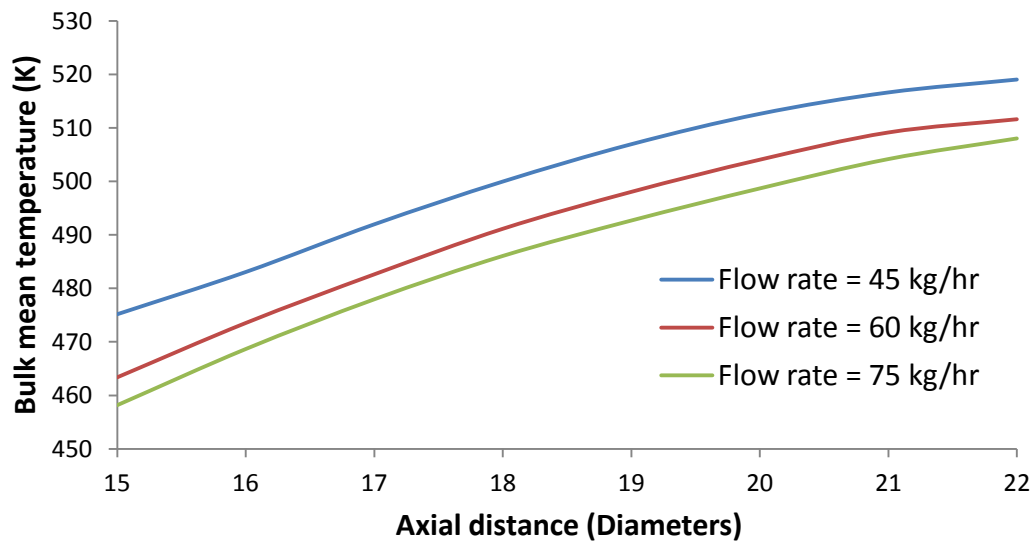


Fig. 4.20 Variation of bulk mean temperature in the metering zone for various flow rates

CHAPTER 5

CONCLUSION AND FUTURE WORK

In this work a detailed numerical analysis of the melting process taking place in the screw of the single screw extruder has been performed. The governing equations for compressible viscous non-Newtonian flow for an unwounded helical channel were solved using Semi Implicit Method for Pressure Linked Equations (SIMPLE) algorithm using an upwind discretization. The model has been verified against the experimental results provided by Altinkaynak et. al. [17]. The results were found in good agreement with the experimental data. The melting process is further studied in detail by investigating the effect of changing the process parameters on the melting. The effect of change in barrel temperature, flow rate and screw speed has been studied.

5.1 Conclusions

- The results predicted by the three dimensional model show that the melting process taking place in the screw extruder follows the Maddock mechanism. Initially a melt film is generated between the barrel and solid bed. Due to cross flow the melt in the melt film is pushed towards the active flight. The melting of solid bed starts from the active flight instead of the barrel wall.
- Significant amount of heat is produced by viscous heating which supports the melting. Viscous heating is affected by the barrel temperature, screw speed and the

feed rate. These parameters have significant effect on melting and the quality of polymer obtained at the end of the extruder.

- As barrel temperature increases, the melting rate decreases. However the temperature of polymer melt is found higher at higher barrel temperature. Depositing polymer at higher temperature results in better surface finish. Hence if melting zone of screw is sufficiently large, high barrel temperature is desirable. However it should not be so high to cause the deterioration of polymer by thermal decomposition.
- Low flow rate results in quick melting process. The bulk mean temperature is also found to be higher at the exit of the metering zone as the flow rate is reduced. Hence low flow rates ensure properly melt and homogenized polymer melt having low viscosity at the end of the metering zone. Again, too low flow rate can raise the temperature of polymer too high causing thermal decomposition of the molecular chains.
- Similar to the barrel temperature, faster screw speeds provide polymer at higher bulk mean temperature at the end of the metering zone. It also takes longer screw lengths to ensure complete melting as faster rates need faster heat supply for melting. However the shear rates are better in this case and provide viscous heat which supports the melting. Fast screw speeds also ensure better cross channel flow and better homogenization of the polymer melt.

5.2 Scope of the future work

- In the present study the screw is considered as adiabatic. However in actual case screw temperature lies between barrel temperature and atmospheric temperature. An experimental study is required to get exact temperature distribution on the screw. Implementing this boundary condition would result in more accurate predictions of melting and metering.
- In the present study, the flight clearance is neglected. In worn out screws a clearance is present and a thin polymer film is present in the clearance. Viscous heating taking

place in that film may add some amount of heat and support the melting process. Hence for more accurate results, the clearance has to be considered.

- The channel is considered as an unwound helix. Helical geometry can be considered to study the effect of radius of curvature.
- An experimental study needs to be done to study the effect of process parameters in actual working conditions.

REFERENCES

- [1] B. V. Reddy, N. V. Reddy, and A. Ghosh, "Fused deposition modelling using direct extrusion," *Virtual Phys. Prototyp.*, vol. 2, no. 1, pp. 51–60, 2007.
- [2] N. Venkataraman, S. Rangarajan, M. J. Matthewson, B. Harper, A. Safari, S. C. Danforth, G. Wu, N. Langrana, S. Guceri, and A. Yardimci, "Feedstock material property process relationships in fused deposition of ceramics (FDC)," pp. 244–252, 1992.
- [3] A. Bellini, L. Shor, and S. I. Guceri, "New developments in fused deposition modeling of ceramics," *Rapid Prototyp. J.*, vol. 11, no. 4, pp. 214–220, 2005.
- [4] Z. Tadmoro and I. Klein, "The Effect of Design and Operating Conditions on Melting in Plasticating Extruders," 1968.
- [5] T. Sastrohartono, Y. Jaluria, M. Essegir, and V. Sernas, "A numerical and experimental study of three-dimensional transport in the channel of an extruder for polymeric materials," *Int. J. Heat Mass Transf.*, vol. 38, no. 11, pp. 1957–1973, 1995.
- [6] B. Maddock, "A Visual Analysis of Flow and Mixing in Extruder Screws," *SPE ANTEC Tech. Pap.*, vol. 15, p. 7, 1959.
- [7] A. P. D. Cox, J. G. Williams, and D. P. Isherwood, "The melting behavior of a low density polyethylene powder in a screw extruder," *Polym. Eng. Sci.*, vol. 21, no. 2, pp. 86–92, 1981.
- [8] D. I. Marshall and I. Klein, "Fundamentals of Plasticating Extrusion - II Experiments," *Polym. Eng. SCIENCE*, 1966.
- [9] Z. Tadmor, I. Duvdevani, and I. Klein, "Melting in plasticating extruders theory and experiments," *Polym. Eng. Sci.*, vol. 7, no. 3, pp. 198–217, 1967.
- [10] F. R. Kulas and N. P. Thorshaug, "PVC Powder Extrusion : Melting Properties and Particle Morphology," vol. 23, pp. 1781–1794, 1979.
- [11] Z. Tadmor and C. G. Gogos, *Principles of Polymer Processing*. 2006.

- [12] E. Mount and C. Chung, "Melting behavior of solid polymers on a metal surface at processing conditions," *Polym. Eng. Sci.*, pp. 1–10, 1978.
- [13] M. Viriyayuthakorn and B. Kassahun, "A three dimensional model for plasticating extrusion screw design.," *SPE-ANTEC Tech. Pap.*, p. 1985, 1985.
- [14] R. M. Griffith, "Fully developed flow in screw extruders," *IEC Fundam.*, vol. 1, no. 3, pp. 180–187, 1962.
- [15] S. Syrjälä, "On The Analysis Of Fluid Flow And Heat Transfer In The Melt Conveying Section Of A Single-Screw Extruder," no. January 1997, pp. 25–48, 1999.
- [16] S. Syrjälä, "A new approach for the simulation of melting in extruders," *Int. Commun. Heat Mass Transf.*, vol. 27, no. 5, pp. 623–634, 2000.
- [17] A. Altinkaynak, M. Gupta, M. A. Spalding, and S. L. Crabtree, "Melting in a single screw extruder: experiments and 3D finite element simulations," *Int. Polym. Process.*, vol. 26, no. 2, pp. 182–196, 2011.
- [18] B. B. Vasudevarao, D. P. Natarajan, and M. Henderson, "Sensitivity of RP Surface Finish to Process Parameter Variation," *Solid Free. Fabr. Proc.*, pp. 251–258, 2000.
- [19] V. Raghavendra Rao, "Analysis of Fluid Flow and Heat Transfer in the Melt Conveying Section of Extrusion Deposition Process," Indian Institute of Technology, Kanpur, 2006.
- [20] D. Horvath, R. Noorani, and M. Mendelson, "Improvement of Surface Roughness on ABS 400 Polymer Using Design of Experiments (DOE)," *Mater. Sci. Forum*, vol. 561–565, pp. 2389–2392, 2007.
- [21] S. H. Ahn, M. Montero, D. Odell, S. Roundy and P. K. Wright, "Anisotropic material properties of fused deposition modeling ABS," *Rapid Prototyp. J.*, vol. 8, no. 4, pp. 248–257, 2002.
- [22] S. Patankar, "Numerical heat transfer and fluid flow," *Series in computational methods in mechanics and thermal sciences*. pp. 1–197, 1980.

- [23] L. W. McKeen, "*Effect of Temperature and Other Factors on Plastics and Elastomers*," 2014.
- [24] M. M. Cross, "Relation between viscoelasticity and shear-thinning behaviour in liquids," *Rheol. Acta*, vol. 18, no. 5, pp. 609–614, 1979.
- [25] C. A. Hieber and H. H. Chiang, "Shear-rate-dependence modeling of polymer melt viscosity," *Polym. Eng. Sci.*, vol. 32, no. 14, pp. 931–938, 1992.
- [26] S. J. Derezinski, "Heat Transfer in Extruder Screws," in *Technical Papers Of The Annual Technical Conference-Society Of Plastics Engineers Incorporated.*, 2000.